1   **Identification of novel antiviral drug candidates using an optimized**

2   **SARS-CoV-2 phenotypic screening platform**

3   Denisa Bojkova[1], Philipp Reus[1,2], Leona Panosch[1], Marco Bechtel[1], Tamara

4   Rothenburger[1], Joshua Kandler[1], Annika Pfeiffer[1], Julian U.G. Wagner[3,4,5], Mariana

5   Shumliakivska[3], Stefanie Dimmeler[3,4,5], Ruth Olmer[6], Ulrich Martin[6], Florian

6   Vondran[7,8], Tuna Toptan[1], Florian Rothweiler[1,9], Richard Zehner[10], Holger Rabenau[1],

7   Karen L. Osman[11], Steven T. Pullan[11], Miles Carroll[11,12,13], Richard Stack[14], Sandra

8   Ciesek[1,2,8], Mark N Wass[14], Martin Michaelis[14]*, Jindrich Cinatl jr.[1,9]*

9

10   [1] Institute of Medical Virology, University Hospital, Goethe-University, Frankfurt am

11   Main, Germany

12   [2] Fraunhofer Institute for Translational Medicine and Pharmacology (ITMP), Frankfurt

13   am Main, Germany

14   [3] Institute for Cardiovascular Regeneration, Centre of Molecular Medicine, Goethe

15   University, Frankfurt am Main, Germany

16   [4] German Center for Cardiovascular Research (DZHK), partner site Rhine-Main,

17   Goethe University, Frankfurt am Main, Germany

18   [5] Cardiopulmonary Institute (CPI), Goethe University, Frankfurt am Main, Germany

19   [6] Leibniz Research Laboratories for Biotechnology and Artificial Organs (LEBAO),

20   Hannover Medical School, Germany

21   [7] Clinic for General, Abdominal and Transplant Surgery, Hannover Medical School,

22   Germany

23   [8] German Center for Infection Research, DZIF, Braunschweig, Germany

24   [9] Dr Petra Joh Research Institute, Frankfurt am Main, Germany

25   [10] Institute for Forensic Medicine, University Hospital, Goethe-University, Frankfurt am

26   Main, Germany

27 [11] Public Health England, National Infection Service, Porton Down, Salisbury, UK

28 [12] Wellcome Trust Centre for Human Genetics, Nuffield Department of Medicine,

29 Oxford University, Oxford, UK

30 [13] NIHR Health Protection Unit in Emerging and Zoonotic Infections, Department of

31 Clinical Infection, Microbiology and Immunology, University of Liverpool, Liverpool, UK

32 [14] School of Biosciences, University of Kent, Canterbury, UK

33

34 *Corresponding authors: Martin Michaelis (M.Michaelis@kent.ac.uk), Jindrich Cinatl jr.

35 (cinatl@em.uni-frankfurt.de)

36

37 **Abstract**

38   Reliable, easy-to-handle phenotypic screening platforms are needed for the

39 identification of anti-SARS-CoV-2 compounds. Here, we present caspase 3/7 activity

40 as a read-out for monitoring the replication of SARS-CoV-2 isolates from different

41 variants, including a remdesivir-resistant strain, and of other coronaviruses in a broad

42 range of cell culture models, independently of cytopathogenic effect formation.

43 Compared to other cell culture models, the Caco-2 subline Caco-2-F03 displayed

44 superior performance, as it possesses a stable SARS-CoV-2 susceptible phenotype

45 and does not produce false-positive hits due to drug-induced phospholipidosis. A

46 proof-of-concept screen of 1796 kinase inhibitors identified known and novel antiviral

47 drug candidates including inhibitors of PHGDH, CLK-1, and CSF1R. The activity of the

48 PHGDH inhibitor NCT-503 was further increased in combination with the HK2 inhibitor

49 2-deoxy-D-glucose, which is in clinical development for COVID-19. In conclusion,

50 caspase 3/7 activity detection in SARS-CoV-2-infected Caco-2F03 cells provides a

51 simple phenotypic high-throughput screening platform for SARS-CoV-2 drug

52 candidates that reduces false positive hits.

53

54

55

Introduction

56

57   There is an ongoing search for antiviral drugs against SARS-CoV-2 that can

58   complement the currently available monoclonal antibody preparations and the three

59   approved small-molecule drugs remdesivir, molnupiravir, and nirmatrelvir [Gao & Sun,

60   2021]. Effective antiviral drugs and drug combinations will be particularly important for

61   immunocompromised individuals, who cannot effectively be protected by vaccination

62   [Gentile & Schiano Moriello, 2022].

63   Previous research has shown that the efficacy of antiviral agents may differ

64   between SARS-CoV-2 variants and cell culture models [Dittmar et al., 2021; Bojkova

65   et al., 2022; Zhao et al., 2022]. Some cell culture models may produce false positive

66   hits due to unspecific effects on the host cell metabolism such as phospholipidosis that

67   do not translate into in vivo activity [Tummino et al., 2021]. Moreover, continued SARS-

68   CoV-2 passaging in cell culture may change virus biology, including virus sensitivity to

69   antiviral drugs [Ogando et al., 2020; Ramirez et al., 2021; Szemiel et al., 2021]. Thus,

70   simple and robust cell culture assays that can cover a broad spectrum of SARS-CoV-

71   2 variants (including primary clinical isolates) are required to accelerate the

72   identification of anti-SARS-CoV-2 drug candidates.

73   Many assays measure SARS-CoV-2-induced host cell destruction (cytopathic

74   effect, CPE) or host cell viability for the identification of antiviral agents [Bojkova et al.

75   2020; Riva et al., 2020; Touret et al., 2020; Zhang et al., 2020; Ellinger et al., 2021;

76   Van Damme et al., 2021; Yan et al., 2021a]. However, such assays are not suitable for

77   SARS-CoV-2 culture systems that do not display virus-induced cytotoxicity [Caccuri et

78   al., 2020; Liao et al., 2020; Bielarz et al., 2021; Wurtz et al., 2021].

79   Antibody-based detection of viral antigens and/ or double-stranded RNA is an

80   alternative approach [Dittmar et al., 2021; Garcia et al. 2021], but requires more

81 manual handling. Assays using genetically modified cells, genetically modified SARS-

82 CoV-2 strains, and SARS-CoV-2 replicons have also been developed [Thi Nhu Tao et

83 al., 2020; Xie et al., 2020; He et al., 2021; Van Damme et al., 2021], but cover only the

84 limited number of virus strains that they have been established for.

85 An ideal assay would enable high throughput screening of wild-type SARS-CoV-

86 2 including the most current clinical isolates in all available cell culture systems in a

87 very simple format that can be applied by many research groups. Such an assay would

88 also enable the phenotypic resistance testing of virus isolates, which is relevant given

89 that the use of antiviral drugs seems to be inevitably associated with the formation of

90 resistant virus variants [Hiscox et al., 2021; Szemiel et al., 2021; Yang et al., 2022].

91 Here, we introduce an effective screening assay for the identification of

92 compounds that inhibit SARS-CoV-2 replication based on measuring caspase 3/7

93 activity using a one-step read-out assay (Caspase-Glo® 3/7 Assay System, Promega).

94 This assay works across different coronaviruses including many SARS-CoV-2 strains

95 and clinical isolates as well as across a broad range of cell culture models, including

96 those in which SARS-CoV-2 infection does not result in a recognizable virus CPE. The

97 Caco-2 subline Caco-2-F03 was identified as preferred cell culture model, as it is easy-

98 to-handle, displays a stable susceptibility phenotype, and does not produce false

99 positives due to drug-induced phospholipidosis. A validation screen of 1796 kinase

100 inhibitors confirmed the suitability of our platform and identified 81 compounds that

101 reduced virus-induced caspase activation by more than 90%, including known as well

102 as novel drug candidates such as PHGDH, CLK-1, and CSFR inhibitors.

103

Results

Caco-2 cells as SARS-CoV-2 infection model

The human colon carcinoma Caco-2 cell line was established by Jorgen Fogh (Memorial Sloan-Kettering Cancer Center, New York) in 1974 [Fogh et al., 1977] and has been used for the cultivation of human pathogenic viruses including influenza viruses and coronaviruses since 1985 [Reigel, 1985; Collins, 1990; Chan et al., 2013a]. We already used Caco-2 cells (obtained from DSMZ, Braunschweig, Germany) for the cultivation of the close SARS-CoV-2 relative SARS-CoV starting in 2003 [Cinatl et al., 2003; Cinatl et al., 2004] and they also enabled us and others to quickly cultivate SARS-CoV-2 isolates when this novel virus emerged [Bojkova et al., 2020; Bojkova et al., 2020a; Bojkova et al., 2020b; Hoehl et al., 2020; Klann et al., 2020; Toptan et al., 2020; Bojkova et al., 2021; Ellinger et al., 2021; Gower et al., 2021; Widera et al., 2021].

In our hands, Caco-2 cells (obtained from DSMZ, Braunschweig, Germany at the time) have been highly permissive to SARS-CoV and SARS-CoV-2 and developed a pronounced cytopathogenic effect (CPE) in response to infection with both viruses [Cinatl et al., 2003; Cinatl et al., 2004; Bojkova et al., 2020b; Bojkova et al., 2021]. In other studies, however, Caco-2 cells displayed low SARS-CoV-2 susceptibility and no CPE formation [Chu et al., 2020; Lee et al., 2020; Yeung et al., 2021].

To further investigate these discrepancies, we ordered fresh Caco-2 cells from the following sources: DSMZ (Braunschweig, Germany, designated as Caco-2A), Sigma (Taufkirchen, Germany, Caco-2B), and CLS (Eppelheim, Germany, Caco-2C). To discriminate our original Caco-2 cell line from these other ones, we will refer to it as Caco-2-F03 from now on.

An initial short tandem repeat (STR) analysis confirmed that all Caco-2 cell lines share the reference profile (Suppl. Table 1). However, Caco-2A, Caco2-B, and Caco-

6

130   2C cells displayed low SARS-CoV-2 permissiveness as indicated by low viral spike (S)

131   protein levels and a lack of CPE formation compared to Caco-2-F03 (Figure 1A, Figure

132   1B).

133

Figure 1
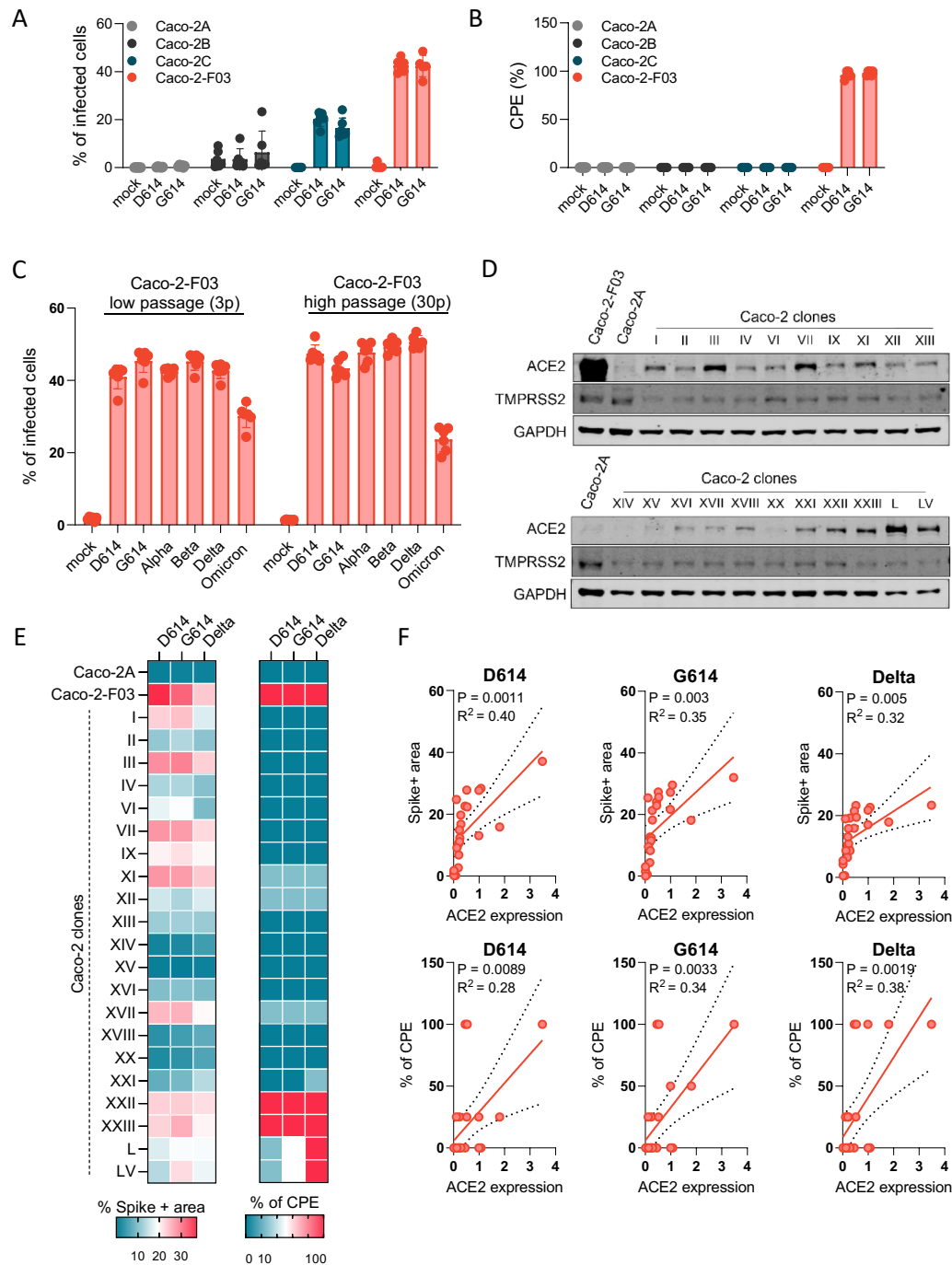
134

135   **Figure 1. Susceptibility of Caco-2 cells to SARS-CoV-2 infection.** A) Percentage

136   of SARS-CoV-2-infected cells detected in Caco-2 cell lines from different sources

7

137   infected with different SARS-CoV-2 isolates at a multiplicity of infection (MOI) 0.01 as

138   determined by immunostaining for the viral spike (S protein) 48h post infection. B)

139   Cytopathogenic effect (CPE) formation in SARS-CoV-2 (MOI 0.01)-infected Caco-2

140   cell lines from different sources as determined 48h post infection. C) Susceptibility of

141   Caco-2-F03 cells to a broad range of SARS-CoV-2 isolates after different times of

142   cultivation. Cells had been frozen at passage 14 and were now resuscitated and

143   cultivated for a further 30 passages. SARS-CoV-2 susceptibility was determined by

144   immunostaining for S 48h after SARS-CoV-2 (MOI 0.01) infection 3 and 30 passages

145   post resuscitation. D) ACE2 and TMPRSS2 levels in Caco-2-F03, Caco-2A, and

146   single-cell derived clones from Caco-2A. E) Susceptibility of Caco-2A clones to

147   selected SARS-CoV-2 isolates as indicated by immunostaining for S and CPE

148   formation in SARS-CoV-2 (MOI 0.01)-infected cells 48h post-infection. F) Correlation

149   of S staining and CPE formation with cellular ACE2 levels.

150

151   Caco-2-F03 cells remained permissive to SARS-CoV-2 for 30 passages after

152   the resuscitation of cells that had been frozen at passage 14 (Figure 1C), suggesting

153   that their SARS-CoV-2 permissiveness phenotype is stable during prolonged culturing.

154   In agreement, we have used Caco-2-F03 cells since 2003 for the cultivation of initially

155   SARS-CoV and later SARS-CoV-2 [Cinatl et al., 2003; Cinatl et al., 2004; Bojkova et

156   al., 2020b; Bojkova et al., 2021].

157   Further investigations revealed that Caco-2-F03 cells display high levels of the

158   cellular SARS-CoV and SARS-CoV-2 receptor ACE2 and the protease TMPRSS2,

159   which cleaves and activates S for ACE2 binding [Hoffmann et al., 2020], than Caco-

160   2A, Caco-2B, and Caco-2C (Figure 1D, Suppl. Figure 1).

161

The Caco-2A cell line contains SARS-CoV-2-susceptible subpopulations

One explanation for these differences between Caco-2-F03 and Caco-2A, Caco-2B, and Caco-2C is that we may have inadvertently enriched a SARS-CoV-2-permissive subpopulation during Caco-2 cultivation. To test this hypothesis, we established 21 single cell-derived clones from Caco-2A by limited dilution. Four of these clonal sublines were highly susceptible to SARS-CoV-2 infection as demonstrated by high S protein levels and CPE formation (Figure 1E), supporting the hypothesis that Caco-2-F03 has been derived from a SARS-CoV- and SARS-CoV-2-permissive subpopulation of our original Caco-2 cell line. There was some level of correlation between the SARS-CoV-2 susceptibility of Caco-2A clones and the cellular ACE2 levels (Figure 1F) but not between SARS-CoV-2 susceptibility and the cellular TMPRSS2 levels (Suppl. Figure 1). This suggests that ACE2 levels are more important for the SARS-CoV-2 susceptibility of Caco-2 cells than TMPRSS2 levels and that additional mechanisms are also likely to be involved.

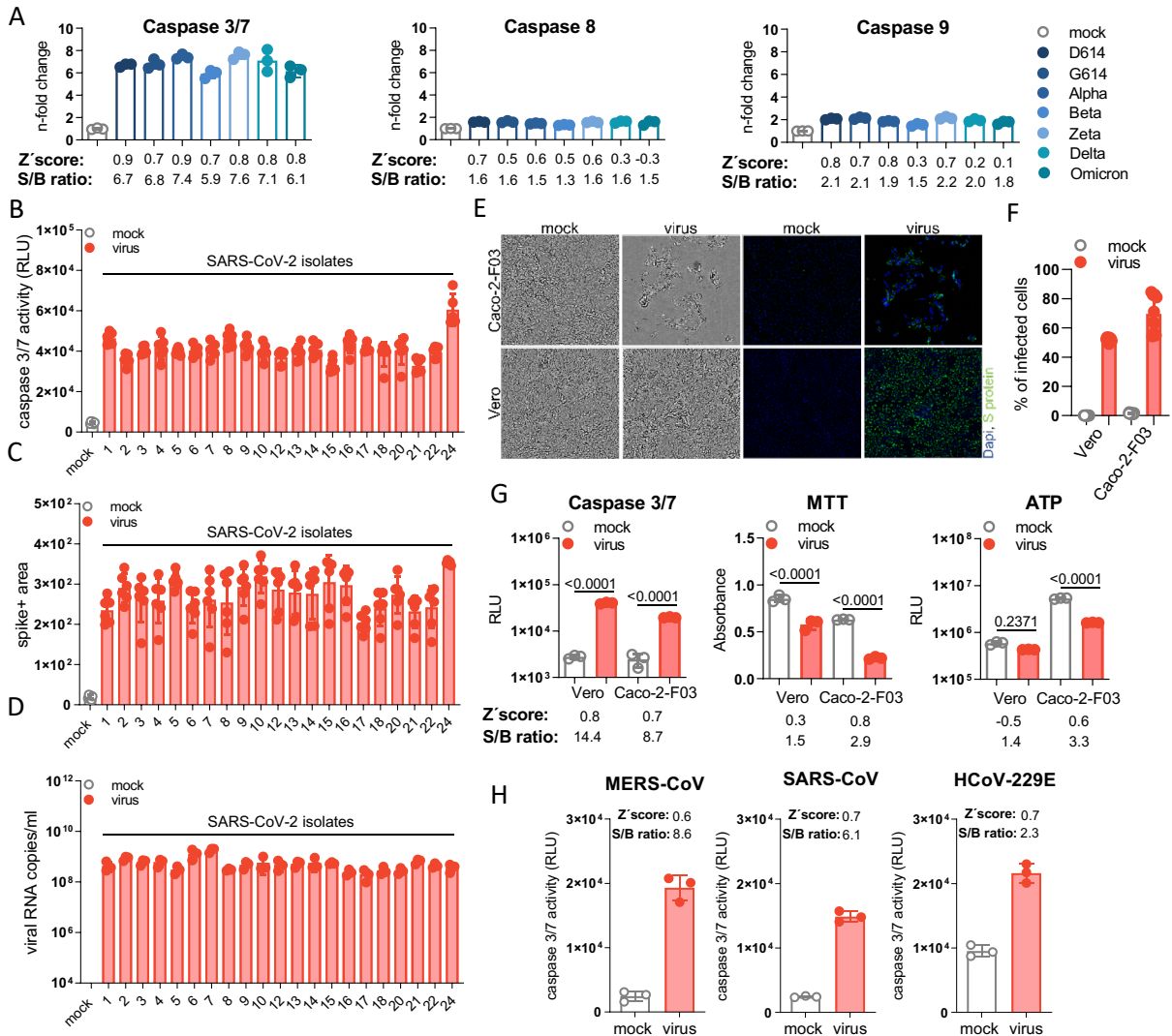**Caspase 3/7 activity for the quantification of the replication of SARS-CoV-2 and other coronaviruses**

Coronavirus replication, including that of SARS-CoV-2, has been shown to result in the activation of caspases including the initiator caspases 8 and 9 and the effector caspase 3 [Conolly & Fearnhead, 2017; Bojkova et al. 2020a; Bojkova et al. 2020b; Li et al., 2020; Ren et al., 2020].

Quantification of caspase activity in Caco-2-F03 cells infected with different SARS-CoV-2 isolates at a multiplicity of infection (MOI) of 0.01 48h post infection using the Caspase-Glo assay kit (Promega) resulted in substantially higher signal-to-basal (S/B) ratios for caspase-3/7 (5.9- to 7.7-fold) than for caspase-8 (1.3- to 1.6-fold) and caspase-9 (1.5- to 2.2-fold) (Figure 2A). Caspase 3/7 activity also resulted in higher Z'

9

188   scores (0.7-0.9) than caspase 8 (0.5-0.7) and caspase 9 (0.3-0.8) activity (Figure 2A),

189   indicating higher assay robustness [Zhang et al., 1999). Hence, caspase 3/7 activity

190   detection was selected for further investigation as potential screening endpoint

191   method.

192

Figure 2

193

Figure 2. Caspase 3/7 activity for the quantification of the replication of SARS-CoV-2 and other coronaviruses. A) Caspase 3/7, caspase 8, and caspase 9 activity in Caco-2-F03 cells infected with a range of different SARS-CoV-2 isolates (MOI 0.01), as determined by Caspase-Glo assay assay (Promega) 48h post infection. Higher signal-to-basal (S/B) ratios and Z' scores indicate higher assay robustness. B)

10

199   Caspase 3/7 activity as determined by Caspase-Glo assay, C) SARS-CoV-2 Spike (S)

200   protein staining, and D) virus titers as indicated by genomic RNA copy numbers

201   determined by qPCR in Caco-2-F03 cells infected with a wide range of uncharacterized

202   SARS-CoV-2 isolates (MOI 0.01) 48h post infection. E) Representative images

203   indicating CPE formation in G614 (MOI 0.01)-infected Caco-2-F03 and Vero cells 48h

204   post infection as indicated by phase contrast microscopy and immunofluoresce

205   staining for the viral S protein in combination with DAPI-stained nuclei. F)

206   Quantification of cellular S protein levels in Caco-2-F03 cells infected with G614 (MOI

207   0.01) 48h post infection by immunostaining. G) Only caspase 3/7 activity but not

208   viability assays (MTT, CellTiter-Glo measuring ATP production) reflects G614 (MOI

209   0.01) replication 48h post infection in Vero cells, which do not display a virus-induced

210   CPE. G614 (MOI 0.01)-infected Caco-2-F03 cells served as a control that displays a

211   CPE. P values were calculated by one-way ANOVA. H) Caspase 3/7 activity in Caco-

212   2-F03 cells infected with MERS-CoV, SARS-CoV, and HCoV-229E (MOI 0.01) as

213   determined 48h post infection including S/B ratios and Z' scores.

214

215   Caspase 3/7 activity displayed an MOI-dependent increase in Caco-2-F03 cells

216   24 h post infection (Suppl. Figure 2A), which mirrored CPE formation (Suppl. Figure

217   2B). 48h post infection, such differences were not detectable anymore (Suppl. Figure

218   2A, Suppl. Figure 2B). Moreover, infection of Caco-2-F03 cells with an additional 21

219   clinical SARS-CoV-2 isolates (after a maximum of two passages in Caco-2-F03 cells)

220   also resulted in effective caspase 3/7 activation (Figure 2B), which reflected viral spike

221   (S) protein levels and virus titers (as indicated by genomic RNA copy numbers) (Figure

222   2C, Figure 2D). UV-inactivated virus did not cause caspase 3/7 activation (Suppl.

223   Figure 2C), further confirming that SARS-CoV-2-induced caspase 3/7 activation

224   depends on virus replication.

225   However, caspase 3/7 activation does not appear to be critically involved in

226   SARS-CoV-2 replication as the clinically approved pan-caspase inhibitor emricasan

227   [Shiffman et al., 2010] did not interfere with SARS-CoV-2 replication and CPE

228   formation, despite suppressing caspase 3/7 activity (Suppl. Figure 3).

229

230   **Caspase 3/7 activity for the monitoring of SARS-CoV-2 replication in the**

231   **presence and absence of a virus-induced cytopathogenic effects (CPE)**

232   The caspase 3/7 assay also enabled the monitoring of SARS-CoV-2 replication

233   in Vero cells, in which SARS-CoV-2 does not induce a CPE and in which SARS-CoV-

234   2 replication cannot be monitored by viability assays such as the MTT assay (measures

235   oxidative phosphorylation in the mitochondria) and the Cell TiterGlo assay (Promega,

236   measures cellular ATP production) (Figure 2E-G).

237

238   **Caspase 3/7-induction by additional coronaviruses**

239   Caspase 3/7 activity also indicated replication of the additional human-

240   pathogenic coronaviruses SARS-CoV, MERS-CoV, and HCoV-229E in CaCo-2-F03

241   cells in Caco-2-F03 cells (Figure 2H).

242

12

243 **Caspase 3/7 activity for the monitoring of SARS-CoV-2 replication in primary**

244 **human cell cultures**

245 Furthermore, SARS-CoV-2-induced caspase 3/7 activity was detected in

246 primary cultures of normal human cells, including induced pluripotent stem cell-derived

247 cardiomyocytes (CMS), air liquid interface (ALI) cultures of bronchial epithelial (HBE)

248 cells, and hepatocytes (PHH) (Suppl. Figure 4A). Immunoblots for the viral

249 nucleoprotein (NP) were used to confirm SARS-CoV-2 infection in these primary cell

250 cultures (Suppl. Figure 4B). ALI HBE did not display disruption of cellular barrier during

251 SARS-CoV-2 infection as measured by transepithelial electrical resistance (TEER) and

252 LDH release (Suppl. Figure 4C and D), whereas CMS and PHH displayed a CPE in

253 response to SARS-CoV-2 infection (Suppl. Figure 4E and F). This is agrees with our

254 previous results that caspase 3/7 activity is a suitable read-out method for monitoring

255 SARS-CoV-2 infection both in the presence and absence of a virus-induced CPE.

256 Taken together, detection of caspase 3/7 activity does not only enable the

257 monitoring of the replication of a wide range of SARS-CoV-2 variants and clinical

258 isolates (and of other coronaviruses). It is also a suitable read-out for SARS-CoV-2

259 replication across many different susceptible permanent cell lines and human primary

260 cultures, independently of whether SARS-CoV-2 induces a CPE in these systems.

261

262 **Caspase 3/7 activity for the identification of antiviral drugs**

263 Next, we compared caspase 3/7 activity and S protein staining for the detection

264 of the antiviral activity of drugs with known efficacy against SARS-CoV-2, including

265 remdesivir (RNA-dependent RNA polymerase (RdRp) inhibitor), EIDD-1931 (active

266 form of molnupiravir that induces 'error catastrophe' in newly produced SARS-CoV-2

267 genomes), ribavirin (broad-spectrum antiviral drug), nirmatrelvir (3C-like protease/

13

268   main protease inhibitor), and nafamostat (TMPRSS2 inhibitor) [Apaydın et al., 2021;

269   Simonis et al., 2021] in SARS-CoV-2 variant G614-infected Caco-2-F03 cells. Both

270   detection methods resulted in very similar IC50s (concentrations that inhibit virus

271   activity by 50%) (Figure 3A).

272

Figure 3
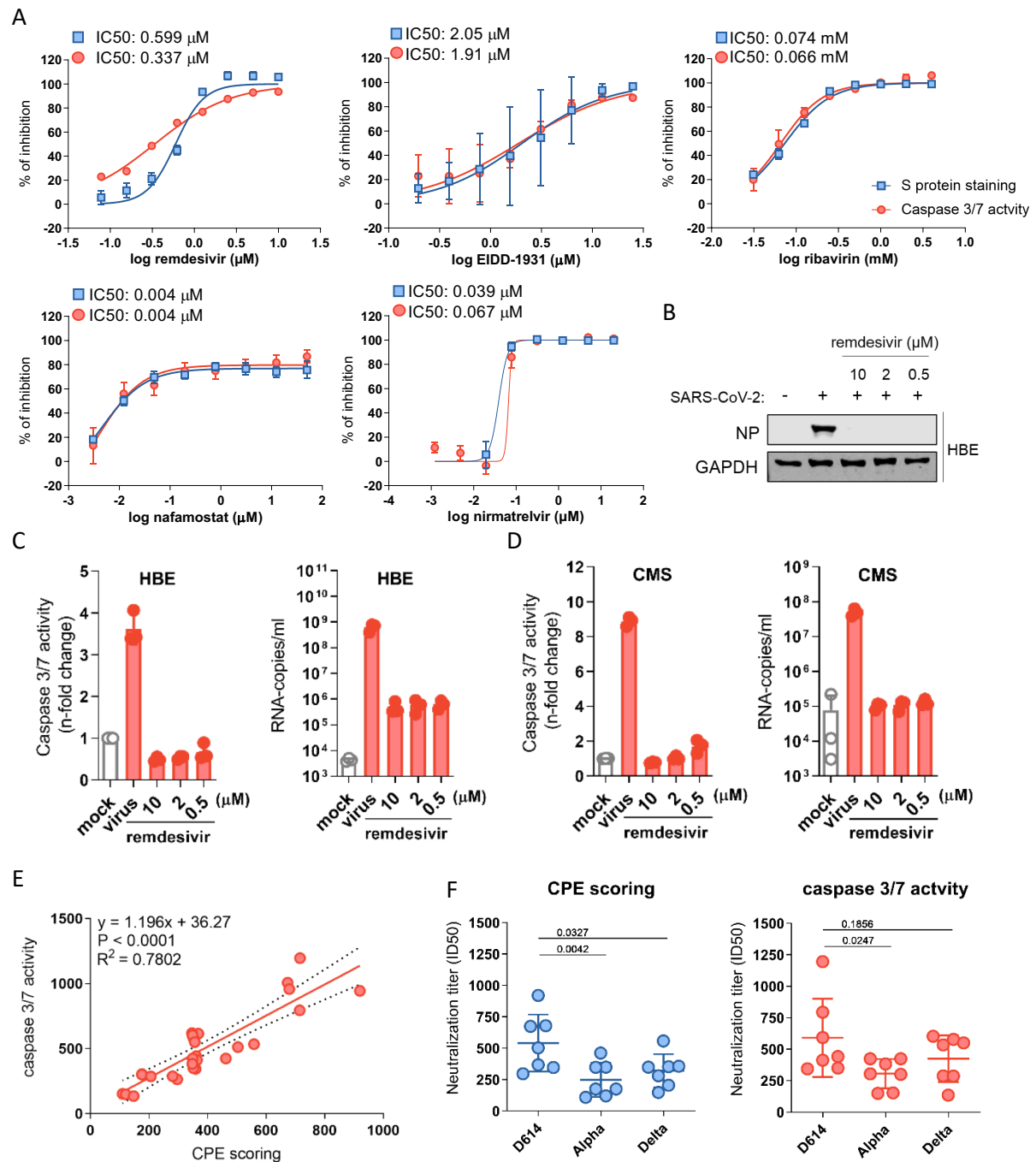
273

274 **Figure 3. Caspase 3/7 activity for the determination of the antiviral activity of**

275 **anti-SARS-CoV-2 agents and neutralization assays**. A) Dose-response curves and

276 concentrations that inhibit virus infection by 50% (IC50) of antiviral agents as

277 determined by caspase 3/7 activity and immunostaining for the coronavirus S protein

278 in G614 (MOI 0.01)-infected Caco-2-F03 cells 24h post infection. B) Effects of the

279 approved anti-SARS-CoV-2 drug remdesivir on cellular levels of the viral NP protein in

280 G614 (MOI 1)-infected air liquid interface (ALI) cultures of primary human bronchial

281 epithelial (HBE) cells 120h post infection. C) Effects of remdesivir on caspase 3/7

282 activity and virus titers (genomic RNA copy numbers determined by PCR) in G614

283 (MOI 1)-infected ALI HBE cultures 120h post infection. D) Effects of remdesivir on

284 caspase 3/7 activity and virus titers in G614 (MOI 1)-infected primary human

285 cardiomyocytes (CMS) 48h post infection. E) Correlation of the neutralization capacity

286 of sera derived from seven donors two weeks after their second dose of the mRNA-

287 1273 vaccine determined by caspase 3/7 activity or cytopathogenic effect (CPE)

288 scoring in D614, Alpha and Delta-infected Caco-2-F03 cells 48h post infection. F)

289 Determination of neutralization titers by caspase 3/7 activity or CPE scoring using sera

290 derived from seven donors two weeks after their second dose of the mRNA-1273

291 vaccine in Caco-2-F03 cells infected with D614, Alpha, and Delta isolates 72h post

292 infection. P values were calculated using paired t-test.

293

294 　　　　Caspase 3/7 activity also enabled the monitoring of the antiviral activity of

295 remdesivir in SARS-CoV-2-infected primary ALI HBE and HNE cell cultures that do not

296 display a recognizable CPE. The validity of the results obtained by caspase 3/7 assay

297 was confirmed by determining virus titers and Western Blot analysis of SARS-CoV-2

298 N protein levels (Figure 3B,C). Finally, caspase 3/7 activity reflected the effect of

299 remdesivir on SARS-CoV-2 replication in CMS (Figure 3D).

300   Taken together, these findings demonstrate that caspase 3/7 activity enables

301   the monitoring of the antiviral drug response in a broad range of cell culture models.

302

303   **Caspase 3/7 activity for the determination of neutralizing antibody titers**

304   Caspase 3/7 activity also enabled the determination of neutralizing antibody

305   titers in sera derived from seven donors two weeks after their second dose of the

306   mRNA-1273 vaccine, as indicated by a close correlation with results obtained by CPE

307   scoring in Caco-2-F03 cells infected with different SARS-CoV-2 variants (Figure 3E,

308   F). The neutralization capacity of the sera was higher against the early SARS-CoV-2

309   strain FFM3 (G614) than against Alpha (B1.1.7) and Gamma (P.2) variant isolates

310   (Figure 3F), which is in line with the immune evasion properties documented for these

311   variants [Zhang et al., 2021].

312

313   **Caspase 3/7 activity for detection of SARS-CoV-2 resistance**

314   Next, we tested whether the caspase 3/7 activity assay may be used for

315   phenotypic screens identifying resistant virus strains. To establish a drug-resistant

316   strain, SARS-CoV-2 strain FFM3 (G614) was passaged in the presence of increasing

317   remdesivir concentrations starting with 0.5 µM (the IC50 concentration) until it could

318   be cultivated in the presence of remdesivir 2µM (FFM3^{r}REM). FFM3^{r}REM displayed a

319   significantly reduced sensitivity to remdesivir, as indicated by determination of cellular

320   S levels in Caco-2-F03 and Calu-3 cells (Figure 4A) and by caspase 3/7 activity in

321   Caco-2-F03 cells (Figure 4B). Interestingly, this remdesivir-resistant strain displayed

322   increased sensitivity to EIDD-1931 and ribavirin relative to the parental strain (Figure

323   4A,B).

324

16
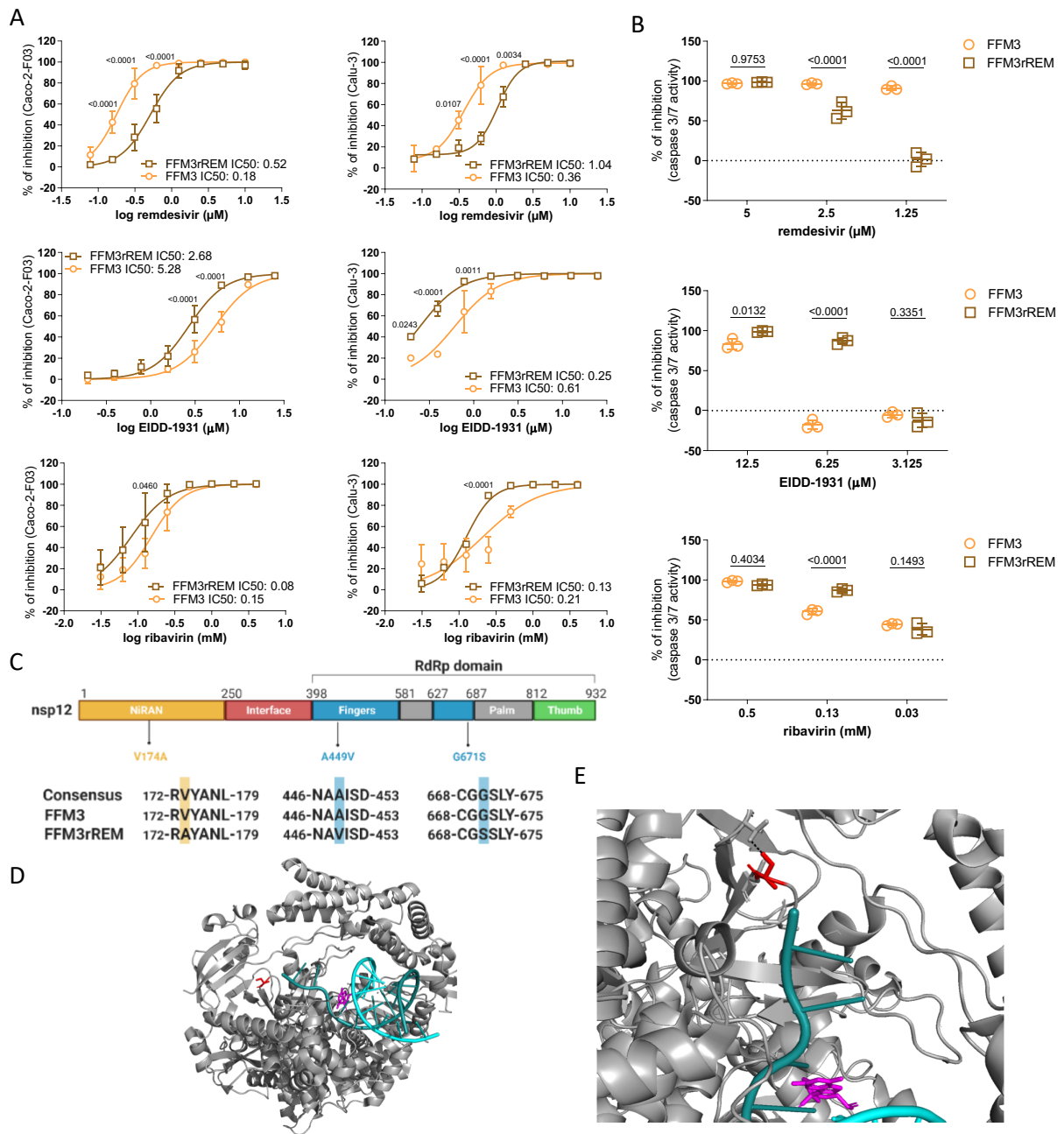
Figure 4

Figure 4. Caspase 3/7 activity for the phenotypic resistance testing of SARS-CoV-2 strains. A) Drug dose response curves and concentrations that reduce cellular levels of the SARS-CoV-2 S protein by 50% (IC50) in Caco-2-F03 and Calu-3 cells as determined by immunostaining 24h (Caco-2-F03) or 48h (Calu-3) post infection with the SARS-CoV-2 strain FFM3 or its remdesivir-adapted substrain FFM3rREM at MOI 0.01. B) Drug concentrations that reduce caspase 3/7 activity in FFM3 and FFM3rREM

17

332   (MOI 0.01)-infected Caco-2-F03 cells 48h post infection. C) Sequence variants in

333   FFM3rREM compared to FFM3. D) The polymerase complex with nsp7 and nsp8 and

334   a template-primer RNA (cyan and deep teal) and remdesivir (magenta) bound.

335   Gly671Ser is shown in red (as serine). E) The SARS-CoV-2 polymerase Gly671Ser

336   sequence variant. Residue 671 is shown in red as serine, which would be able to form

337   a hydrogen bond with Thr402 which would not be present as Gly671. All p values were

338   calculated by two-way ANOVA.

339

340   Sequencing of FFM3^{r}REM identified a 154452G>A mutation (present in >90%

341   of alleles) in the coding region of the RNA-dependent RNA polymerase, which results

342   in a change from glycine to serine in position 671(Gly671Ser) (Figure 4C). Gly671Ser

343   is located in the polymerase domain of the RNA-dependent RNA polymerase in close

344   vicinity to where RNA leaves (or enters) the active site (Figure 4D). Gly671Ser could

345   have an effect on the protein structure, as it is located in a bend between two beta

346   sheets, where glycine often has an important role. Additionally, Gly671Ser introduces

347   a side chain capable of forming a hydrogen bond with Thr402 on an adjacent loop

348   (Figure 4E), which could have an effect on the flexibility and conformation of the

349   protein. Therefore, Gly671Ser seems likely to reduce either the binding affinity for

350   remdesivir or to enable the polymerase to overcome the effect of the drug.

351   Although our structural analysis plausibly explains why Gly671Ser in the RNA-

352   dependent RNA polymerase is likely to mediate remdesivir resistance, it would have

353   been impossible to determine this as a resistance variant without the prior knowledge

354   that the change had happened in response to SARS-CoV-2 adaptation to remdesivir.

355   Hence, this finding emphasizes the relevance of phenotypic assays for the

356   identification of resistant strains that cannot be identified by the analysis of viral

357   genomic information and the subsequent elucidation of the underlying resistance

18

358   mechanisms. Notably, the caspase 3/7 activity assay also provides an easy-to-use

359   read-out for such phenotypic virus resistance testing approaches.

360

361   **Comparison of Caco-2F03 with other cell line candidates for the identification of**

362   **anti-SARS-CoV-2 drug candidates in screening assays**

363   Next, we directly compared Caco-2F03 to other SARS-CoV-2 cultivation models

364   that could be used for the identification of anti-SARS-CoV-2 drug candidates in

365   screening assays. We focused on permanent cell lines that are easy to cultivate and

366   maintain.

367   Suitable cell line candidates should be highly permissive for a broad spectrum

368   of SARS-CoV-2 variants and display high caspase 3/7 activity upon infection. We had

369   already shown that Caco-2-F03 cells display high susceptibility to a broad range of

370   SARS-CoV-2 isolates (Figure 2). Here, we directly compared the susceptibility of

371   A549-ACE2, Calu-3, Vero, and Caco-2-F03 cells to D614, G614, Alpha, Beta, and

372   Delta isolates. S immunostaining and caspase 3/7 activity showed that Caco-2-F03

373   displayed the most pronounced broad-spectrum permissiveness to all tested SARS-

374   CoV-2 isolates (Suppl. Figure 5A, 5B).

375   Recently, drug-induced phospholipidosis was demonstrated to affect antiviral

376   screens by causing false positive hits due to unspecific effects that do not translate

377   into the clinical setting [Tummino et al., 2021]. In particular, cationic amphiphilic drugs

378   such as hydroxychloroquine were found to induce phospholipidosis [Tummino et al.,

379   2021]. Hence, SARS-CoV-2 culture systems for phenotypic antiviral screening would

380   ideally avoid false positives due to phospholipidosis.

381   Treatment with hydroxychloroquine resulted in considerable phospholipidosis

382   and inhibited a Delta isolate in A549-ACE2 and Vero cells but not in Calu-3 or CaCo-

383   2-F03 cells (Suppl. Figure 5C, 5D). Due to the susceptibility to the broadest range of

384   SARS-CoV-2 isolates and the insensitivity to drug-induced phospholipidosis, we

385   selected Caco-2-F03 cells for a proof-of-concept screen for anti-SARS-CoV-2 drug
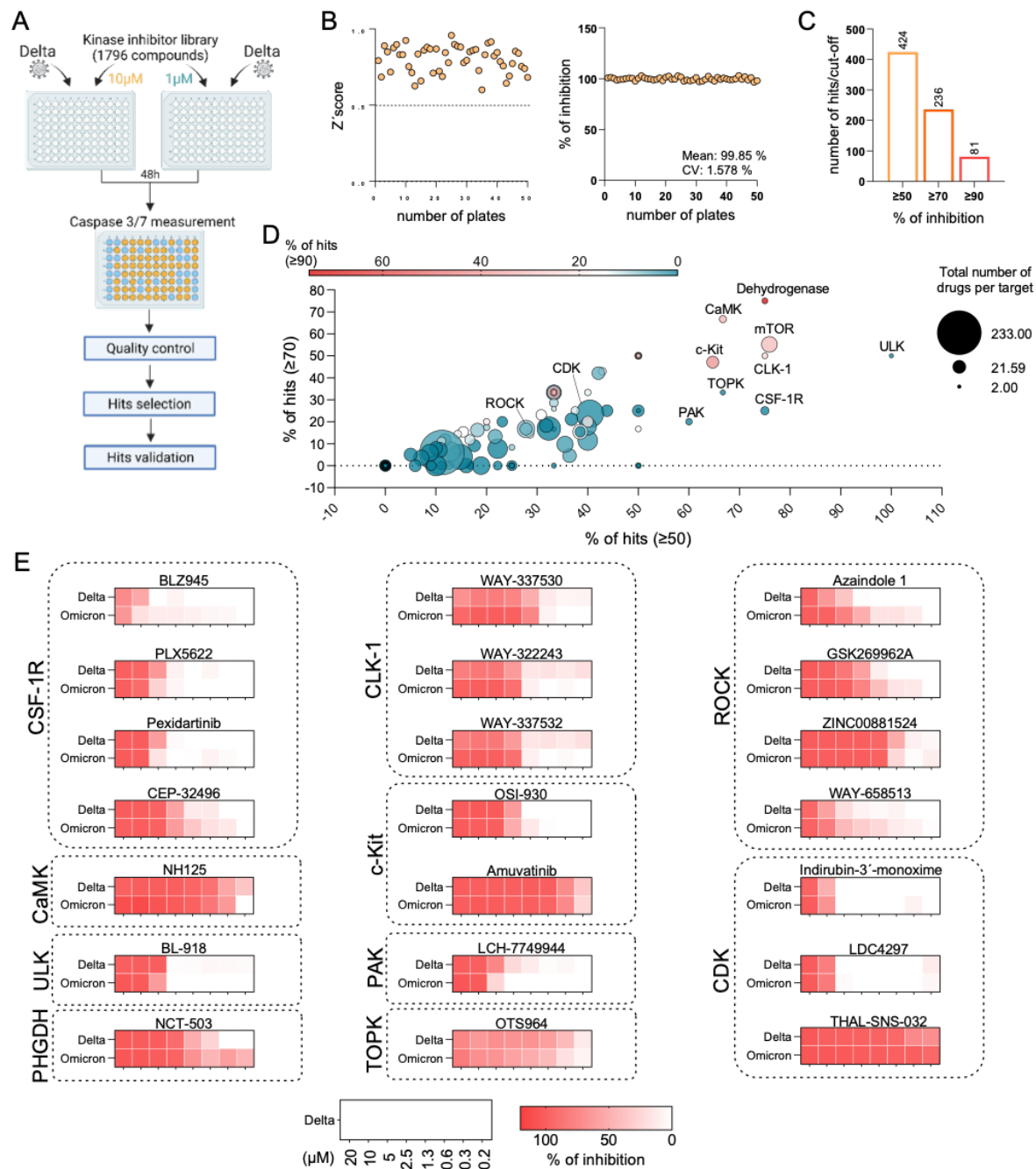
386   candidates.

387

388   **Proof-of-concept kinase inhibitor screen for drug candidates that inhibit SARS-**

389   **CoV-2 replication**

390   Next, we used the caspase 3/7 activity assay in Caco-2F03 cells to screen the

391   Kinase Inhibitor Library (96-well)-L1200 (Selleck) for anti-SARS-CoV-2 drug

392   candidates (Figure 5A, Suppl. File 1). All compounds were tested at a concentration of

393   10µM. Z'scores were determined as quality controls on all plates as previously

394   described [Xu et al., 2016], and only plates with a Z´score ≥ 0.5 were further analyzed

395   (Figure 5B). Moreover, remdesivir (10 µM) was used as positive control on each plate

396   and produced consistent results (Figure 5B).

397

Figure 5

398

Figure 5. Proof-of-concept screen for anti-SARS-CoV-2 drug candidates using the Caco-2-F03 cell line platform and caspase 3/7 activity as read-out method. A) Overview of the proof-of-concept screen for anti-SARS-CoV-2 compounds using the Kinase inhibitor library L-1200 (Selleckchem, Germany) containing 1796 compounds (Selleckchem, Germany) in Delta (MOI 0.01)-infected Caco-2-F03 cells using caspase 3/7 activity as read-out 48h post infection. For the screen, every compound was tested

405   at a concentration of 10 and 1 µM. 21 selected hits were then confirmed by determining

406   drug-response curves. B) Quality controls, Z'scores served as quality controls (left).

407   Only plates with a Z´score ≥ 0.5 were further analyzed. Remdesivir (10 µM) was used

408   as positive control on each plate and produced consistent results (right). C) Number of

409   hits at different inhibition cut-offs. D) Visualization of the distribution of hits according

410   to their targets. Targets for which inhibitors were selected for confirmation are

411   indicated. E) Heatmaps of the anti-SARS-CoV-2 activity of 21 hits by the determination

412   of dose-response in Delta and Omicron (MOI 0.01)-infected Caco-2-F03 cells using

413   immunostaining for the viral S protein as read-out 24h post infection.

414

415   All compounds were tested at a concentration of 10µM, which resulted in 81

416   hits, when we considered $\geq$ 90% inhibition of caspase 3/7 activity as a cut-off (Figure

417   5C). Most hits were identified among inhibitors that target dehydrogenases, CaMK,

418   mTOR, ULK, CLK-1, TOPK, CSF-1R, and PAK (Figure 5D). CaMK, mTOR, ULK,

419   TOPK (also known as PBK), and PAK had already been proposed as antiviral drug

420   targets for SARS-CoV-2 [Shahinozzaman et al., 2020; Jamaly et al., 2021; Shang et

421   al., 2021; Agrawal et al., 2022; Basile et al., 2022]. However, we could not find any

422   information on potential anti-SARS-CoV-2 effects caused by CLK-1 or CSF-1R

423   inhibition. We also included the phosphoglycerate dehydrogenase (PHGDH) inhibitor

424   NCT-503 [Pacold et al., 2016; Hamanaka et al., 2018] in our confirmation experiments.

425   Although dehydrogenases had been known to contribute to SARS-CoV-2 replication

426   [Shang et al., 2021], PHGDH had not previously been shown to be involved.

427   In addition to inhibitors of the targets described above, ROCK and CDK

428   inhibitors were also included into the confirmation experiments. ROCK was described

429   to be involved in the SARS-CoV-2-induced suppression of the host cell interferon

430   response [Zhang et al., 2021a]. CDK inhibitors had previously been shown to inhibit

431   SARS-CoV-2 replication [Gutierrez-Chamorro et al., 2021; Hahn et al., 2021]. The

432   determination of dose-response curves for all of the 21 inhibitors using immunostaining

433   for the SARS-CoV-2 S protein confirmed the results of the screen (Figure 5E, Suppl.

434   Figure 6).

435

PHGDH inhibitor NCT-503 as anti-SARS-CoV-2 drug candidate

437   Since PHGDH is a new potential antiviral drug target for the treatment of SARS-

438   CoV-2 infection, we further investigated NCT-503. To investigate whether PHGDH

439   inhibition is critical for NCT-503-mediated SARS-CoV-2 inhibition, we compared its

440   effects and those of a chemically closely related analogue, which does not inhibit

441   PHGDH and is commonly used as inactive NCT-503 control (Suppl. Figure 7A) [Pacold

442   et al., 2016; Arlt et al., 2021], for antiviral activity. Only NCT-503 but not the inactive

443   control inhibited Delta- and Omicron-induced caspase 3/7 activation indicating that the

444   antiviral effects of NCT-503 are indeed mediated by PHGDH inhibition (Suppl. Figure

445   7B).

446

Figure 6
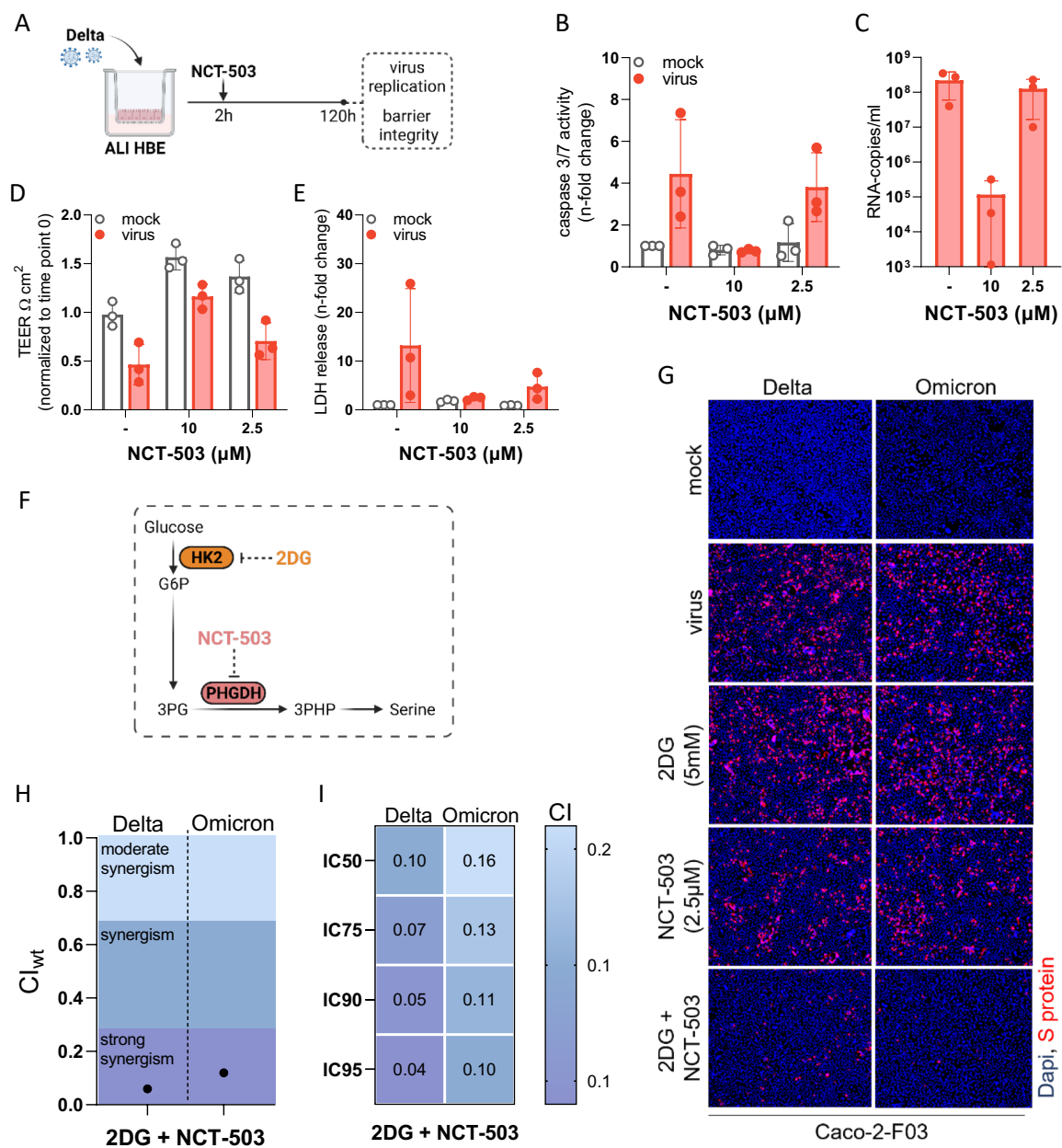
Figure 6. Investigation of the anti-SARS-CoV-2 effects of the PHGDH inhibitor NCT-503 alone or in in combination with 2-Deoxy-D-glucose (2DG). A) Scheme of the testing of NCT-503 for anti-SARS-CoV-2 activity in air liquid interface (ALI) cultures of primary human bronchial epithelial (HBE) cells. Effect of NCT-503 on (B) caspase 3/7 activity, (C) virus titers (determined as genomic RNA copy numbers by qPCR), (D) transepithelial electrical resistance (TEER), and (E) LDH release in ALI HBE cultures infected with Delta (MOI 1) 120h post infection. F) Anti-SARS-CoV-2 effects of NCT-

455   503 in combination with 2-Deoxy-D-glucose (2DG). Illustration of how NCT-503 and

456   2DG can exert combined effects on a common metabolic pathway. G) Representative

457   fluorescence images indicating the number of Delta and Omicron (MOI 0.01)-infected

458   cells in NCT503 and/ or 2DG-treated Caco-2-F03 cultures 24h post infection. H) and

459   I) Weighted combination indices (CIwt) determined by the method of Chou and Talalay

460   [Chou, 2006] indicating a strong synergism of NCT-503 and 2DG.

461

462   NCT-503 also inhibited SARS-CoV-2 replication in primary human bronchial

463   epithelial cell air-liquid interface (ALI) cultures (Figure 6A) as indicated by SARS-CoV-

464   2-induced caspase 3 activity (Figure 6B), viral titers (determined as copy numbers of

465   genomic RNA by PCR) (Figure 6C), cell layer integrity (Figure 6D), and lack of SARS-

466   CoV-2-induced cytotoxicity (as indicated by LDH release) (Figure 6E).

467   Taken together, NCT-503 is a novel antiviral drug candidate for the treatment of

468   SARS-CoV-2 infections that inhibits virus replication via PHGDH inhibition and is

469   effective in different model systems including primary human bronchial epithelial cell

470   ALI cultures, the system considered to be most physiologically relevant [Mulay et al.,

471   2021].

472

473   **NCT-503 in combination with 2-Deoxy-D-glucose (2DG)**

474   The discovery of PHGDH as novel antiviral drug target and of NCT-503 as

475   antiviral drug candidate offers potential additional opportunities for combination

476   therapies that display higher efficacy than either single treatment.

477   *De novo* serine synthesis is a side branch of glycolysis that includes the

478   conversion of the glycolytic intermediate 3-phosphoglycerate (3PG) into 3-

479   phosphohydroxypyruvate (3PHP) by PHGDH (Figure 6F) [Geeraerts et al., 2021]. The

480   production of 3PG in the glycolytic cycle depends on the phosphorylation of glucose

25

481   into glucose-6-phosphate (G6P) by hexokinase II (HK2) as an initial step (Figure 6F)

482   [Pajak et al., 2020]. Notably, the HK2 inhibitor 2-Deoxy-D-glucose (2DG) has already

483   been shown to inhibit SARS-CoV-2 replication [Bojkova et al., 2020; Bojkova et al.,

484   2021a]. Hence, we hypothesized that the combined inhibition of *de novo* serine

485   synthesis by 2DG and NCT-503 may result in further enhanced antiviral effects (Figure

486   6F).

487   Indeed, the combination of 2DG and NCT-503 resulted in stronger Delta and

488   Omicron BA.1 inhibition than either drug alone (Figure 6G, Suppl. Figure 7C). The

489   determination of combination indices (CIs) by the method of Chou and Talalay [Chou,

490   2006] indicated a strong synergism of NCT-503 and 2DG against both SARS-CoV-2

491   isolates (Figure 6H, Figure 6I).

492

493

Discussion

Here, we developed a novel screening assay for the identification of anti-SARS-CoV-2 compounds, based on using caspase 3/7 activity determined by the Caspase-Glo® Assay System as read-out indicating SARS-CoV-2 replication. This one step read-out assay can be used by the large number of laboratories, which are equipped with the required plate readers that are in common use. Moreover, the assay is widely (potentially universally) applicable to different SARS-CoV-2 strains and clinical isolates as well as cell culture systems, as indicated by our wide range of pilot experiments. Moreover, our findings show that caspase 3/7 activity can also be used to determine SARS-CoV-2 replication in neutralization assays determining the antibody response in the plasma of individuals and for the phenotypic resistance testing of virus variants. Notably, the caspase 3/7 assay also detects SARS-CoV-2 replication in cultivation systems that do not develop a CPE and in which viability assays such as the MTT assay and the Cell Titer Glo® Assay did not reflect SARS-CoV-2 replication.

For our proof-of-concept experiment for phenotypic resistance testing, we established a remdesivir-resistant SARS-CoV-2 strain by adapting the SARS-CoV-2 strain FFM3 to replication in the presence of remdesivir. Our results confirmed previous observations [Szemiel et al., 2021; Yang et al., 2022] demonstrating that SARS-CoV-2 resistance formation against clinically approved antiviral drugs poses a relevant risk. Notably, the genetic sequence of our remdesivir-adapted SARS-CoV-2 strain would not have enabled us to identify this as a resistant strain by a genotypic approach, which emphasizes the potential need for effective phenotypic resistance testing platforms in the future.

In addition to identifying an easy-to-handle read-out assay for anti-SARS-CoV-2 agent screens, we were also interested in identifying a well-suited cell culture platform. We considered permanent cell lines to be the most promising candidates,

520   because they are readily available and require a minimum of handling. A number of

521   continuous cell lines (e.g. A549-ACE, Calu-3, Vero, Caco-2) had already been used in

522   different phenotypic screening approaches for the identification of antiviral drug

523   candidates against SARS-CoV-2 [Dittmar et al., 2021; Ellinger et al., 2021; Xu et al.,

524   2021]. Based on our comparison of different candidate cell lines, however, we

525   identified Caco-2-F03 as the best platform, as it displayed susceptibility to the widest

526   range of SARS-CoV-2 strains and isolates and was not affected by drug-induced

527   phospholipidosis that has been shown to result in false-positive hits during the testing

528   of anti-SARS-CoV-2 drug candidates [Tummino et al., 2021].

529   Notably, Caco-2 cells were (in contrast to Calu-3, A549, or Vero cells) shown to

530   be highly susceptible to seasonal coronaviruses such as HCoV-229E or HCoV-OC43

531   [Collins, 1990; Tang et al., 2005; Yoshikawa et al., 2010; Michaelis et al., 2011; Chan

532   et al., 2013; Ramani et al., 2021]. In this context, we found here that the caspase 3/7

533   assay also enabled the monitoring of HCoV-229E replication in Caco-2-F03 cells,

534   indicating that this may also serve as a unique broad-spectrum drug screening platform

535   for (seasonal) coronaviruses.

536   Our study also provided an explanation for the contradictory findings on the

537   SARS-CoV-2 susceptibility of Caco-2 cells reported in previous studies [Bojkova et al.,

538   2020; Bojkova et al., 2020b; Chu et al., 2020; Hoehl et al., 2020; Klann et al., 2020;

539   Lee et al., 2020; Toptan et al., 2020; Bojkova et al., 2021; Ellinger et al., 2021; Gower

540   et al., 2021; Widera et al., 2021; Yeung et al., 2021]. When we investigated newly

541   acquired Caco-2 cell lines from different providers (DSMZ, CLS, Sigma) for SARS-

542   CoV-2 susceptibility, they did indeed not present the level of SARS-CoV-2

543   permissiveness that we find in our Caco-2-F03 cell line. The subsequent analysis of

544   21 clonal sublines of the newly purchased lowly SARS-CoV-2-susceptible Caco-2 cell

545   line from DSMZ (Caco-2A) resulted in a broad range of susceptibility phenotypes,

546   suggesting that a highly SARS-CoV-2-susceptible subpopulation has inadvertently

547   become the dominant population in our Caco-2-F03 cell line. Notably, the susceptibility

548   phenotype of Caco-2-F03 appears to be stable, as we have used this cell line for the

549   cultivation of SARS-CoV and SARS-CoV-2 since 2003 [Cinatl et al., 2003; Cinatl et al.,

550   2004]. Moreover, the SARS-CoV-2 susceptibility phenotype of Caco-2-F03 was

551   maintained for a further 30 passages within the current study. Notably, such phenotypic

552   differences between samples of the same cell line obtained from different sources is

553   not surprising and has been described for different cell lines [Feichtinger et al., 2016;

554   Ben-David et al., 2018; Liu et al., 2019].

555   Next, we used the caspase 3/7 activity assay in Caco-2-F03 cells to screen the

556   Kinase Inhibitor Library (96-well)-L1200 (Selleck) for anti-SARS-CoV-2 drug

557   candidates, which resulted in 81 hits that reduced SARS-CoV-2-induced caspase 3/7

558   activity by $\geq$ 90%. These hits included inhibitors of known potential anti-SARS-CoV-2

559   drug targets (CaMK, mTOR, ULK, TOPK, PAK, ROCK, CDK) [Shahinozzaman et al.,

560   2020; Jamaly et al., 2021; Ellinger et al., 2021; Shang et al., 2021; Zhang et al., 2021b;

561   Agrawal et al., 2022; Basile et al., 2022] and those that interfere with drug targets that

562   had not previously been identified to be relevant during SARS-CoV-2 replication (CLK-

563   1, CSF-1R). We determined dose response curves for 21 out of these 81 hit

564   compounds using immunostaining for the viral S protein, which confirmed their anti-

565   SARS-CoV-2 activities.

566   Among these hits, we further investigated the phosphoglycerate dehydrogenase

567   (PHGDH) inhibitor NCT-503 [Pacold et al., 2016; Hamanaka et al., 2018], as it

568   interferes with a dehydrogenase that had not previously been shown to be involved in

569   SARS-CoV-2 replication. In addition to NCT-503, we tested a structurally closely

570   related analogue that does not inhibit PHGDH [Pacold et al., 2016; Arlt et al., 2021].

571   This inactive NCT-503 analogue did not affect SARS-CoV-2 replication, indicating that

572   the anti-SARS-CoV-2 effects of NCT-503 are caused by its effect on PHGDH.

573   PHGDH activity is critically involved in *de novo* serine synthesis [Geeraerts et

574   al., 2021], a pathway downstream of the glycolytic cycle that depends on the

575   phosphorylation of glucose into glucose-6-phosphate (G6P) by hexokinase II (HK2) as

576   initial step [Pajak et al., 2020]. Since the HK2 inhibitor 2-Deoxy-D-glucose (2DG) has

577   already been shown to inhibit SARS-CoV-2 replication [Bojkova et al., 2020; Bojkova

578   et al., 2021a], we tested whether the combined interference with this pathway using

579   NCT-503 and 2DG resulted in further increased antiviral effects. Indeed, the

580   combination resulted in strongly synergistic anti-SARS-CoV-2 activity. Such antiviral

581   combination therapies have been suggested to be of critical importance for the

582   sustained control of virus outbreaks, as they are not only more effective but also

583   anticipated to reduce and, ideally, prevent resistance formation [White et al., 2021].

584   In conclusion, we here present a novel phenotypic screening platform for the

585   identification of drug candidates with activity against SARS-CoV-2 and other

586   coronaviruses based on the determination of caspase 3/7 activity using the one-step

587   Caspase-Glo® 3/7 Assay System as read-out. Caspase 3/7 activity is also a suitable

588   read-out for neutralization assays and phenotypic resistance testing. The Caco-2-F03

589   cell line was identified as the best-suited cell culture platform. It is susceptible to a

590   particularly broad range of SARS-CoV-2 isolates and its susceptibility phenotype

591   remains stable over many passages. Moreover, Caco-2-F03 is not affected by

592   phospholipidosis, which is known to cause false-positive hits during the testing of

593   potential anti-SARS-CoV-2 agents [Tummino et al., 2021]. Hence, the determination

594   of caspase 3/7 activity in SARS-CoV-2-infected Caco-2-F03 cells represents a newly

595   established screening platform that is easy-to-use also for groups without experience

596   in drug discovery projects. A proof-of-concept screen of a kinase inhibitor library

597   containing 1796 compounds resulted in known and novel anti-SARS-CoV-2 drug

598   targets. The PHGDH inhibitor NCT-503 was identified as novel antiviral drug

599   candidate, whose activity was further increased by 2DG (an inhibitor of the PHGDH

600   upstream HK2), which is under clinical development for the treatment of COVID-19

601   treatment [Sahu & Kumar, 2021].

602

603

Material and methods

Cell culture

Caco-2A (DSMZ), Caco-2B (Sigma), Caco-2C (CLS), Vero (DSMZ), Calu-3 (ATCC), and Caco-2-F03 (Resistant Cancer Cell Line collection, https://research.kent.ac.uk/industrial-biotechnology-centre/the-resistant-cancer-cell-line-rccl-collection/) were grown at 37 °C in minimal essential medium (MEM) supplemented with 10% fetal bovine serum (FBS), 100 IU/mL penicillin, and 100 µg/mL streptomycin. All culture reagents were purchased from Sigma. A549-ACE2 (Invivogen) was grown in DMEM supplemented with 10% FBS, 2% L-glutamine, 100 µg/ml normocin, 0.5 µg/ml puromycin, 100 IU/mL penicillin, and 100 µg/mL of streptomycin. All cell lines were regularly authenticated by short tandem repeat (STR) analysis and tested for mycoplasma contamination.

Primary bronchial epithelial cells were isolated from the lung explant tissue of a patient with lung emphysema as previously described [van Wetering et al., 2000]. For differentiation into air-liquid interface (ALI) cultures, cells were resuscitated, passaged once in PneumaCult-Ex Medium (StemCell technologies), and seeded on transwell inserts (12-well plate, Sarstedt) at 4×10^4 cells/insert. After reaching confluence, medium on the apical side of the transwell insert was removed and medium in the basal chamber was replaced with PneumaCult ALI Maintenance Medium (StemCell Technologies) including Antibiotic/Antimycotic solution (Sigma Aldrich) and MycoZap Plus PR (Lonza). Criteria for successful differentiation were the development of ciliary movement, an increase in transepithelial electric resistance, and mucus production.

Human induced pluripotent stem cell-derived cardiomyocytes (hiPS-CMs) of two donors were obtained with an embryoid body-based protocol as previously described [Breckwoldt et al., 2017]. hiPS-CMs were cultured in RPMI/B27 medium at 37 °C and 5 % CO2 for 4 to 5 days prior to viral infection.

32

630   Primary human hepatocytes (PHHs) were isolated as previously described

631   [Vondran et al., 2008] and were maintained in William's Medium E (PAN Biotech,

632   Aidenbach, Germany) containing 10% fetal bovine serum (Biochrom, Cambridge, UK)

633   and 10,000 U penicillin/streptomycin, 1% L-glutamine, 1% non-essential amino-acids,

634   5mmol/L Hepes (Thermo Fisher Scientific, Schwerte, Germany), 2% dimethyl sulfoxide

635   (DMSO, Roth, Karlsruhe, Germany), 5 µg/mL insulin, and 0.05 mmol/L hydrocortisone

636   (Sigma Aldrich, Munich, Germany).

637

Virus preparation and infection of different cell types

639   Caco-2-F03 cells were used for the isolation SARS-CoV-2 variants applied in this

640   study. Information on the following isolates is available from GenBank: D614 (SARS-

641   CoV-2/FFM1, MT358638), G614 (SARS-CoV-2/FFM7, MT358643), Alpha (SARS-

642   CoV-2/FFM-UK7931/2021, MZ427280), Beta (SARS-CoV-2/FFM-ZAF1/2021,

643   MW822592), Delta (SARS-CoV-2/FFM-IND8424/2021, MZ315141), Zeta (SARS-CoV-

644   2/FFMBRA1/2021, MW822593), Omicron (SARS-CoV-2/FFM-SIM0550/2021,

645   OL800702). Additional isolates were not further characterized. SARS-CoV-2 stocks

646   were cultivated for a maximum of three passages in Caco-2-F03 cells and stored at –

647   80°C. SARS-CoV stocks were prepared on Caco-2-F03 cells as previously described

648   [Cinatl et al., 2004]. MERS-CoV was obtained from BEI Resources (EMC/2012, NR-

649   44260) and passaged once on Vero cells prior experiments. Viral stocks of HCoV-229E

650   (ATCC no. CCL-137) were prepared using Caco-2-F03 cells. Virus titers were

651   determined as TCID50/mL in confluent cells in 96-well microtiter plates.

652   Primary bronchial and nasal epithelial cells in ALI cultures were infected with

653   SARS-CoV-2 from the apical site. The inoculum was incubated for 2 h, then removed

654   and cells were washed three times with PBS. For testing of antiviral activity of drugs,

655 the compounds were added after the infection period from both the apical and the basal

656 site. The apical medium was removed after one day.

657

658 **Caspase activity assay**

659 Caspase 3/7, 8 and 9 activity was measured using the Caspase-Glo assay kit

660 (Promega, Madison, WI, USA), according to the manufacturer's instructions. Briefly,

661 100 µL of Caspase-Glo reagent were added to each well, mixed, and incubated at room

662 temperature for 30 min. Luminescence intensity was measured using an Infinite M200

663 microplate reader (Tecan).

664

665 **Viability assay**

666 Cell viability was measured by 3-(4,5-dimethylthiazol-2-yl)-2,5-

667 diphenyltetrazolium bromide (MTT) dye reduction assay. 25 µL of MTT solution (2

668 mg/mL in PBS) were added per well, and the plates were incubated at 37 °C for 4 h.

669 After this, the cells were lysed using 100 µL of a buffer containing 20% sodium

670 dodecylsulfate and 50% *N*,*N*-dimethylformamide with the pH adjusted to 4.7 at 37 °C

671 for 4 h. Absorbance was determined at 560 nm (reference wavelength 620 nm) using

672 a Tecan infinite M200 microplate reader (TECAN).

673 Alternatively, cell viability was determined using the CellTiter-Glo (Promega),

674 which measures ATP production, according to the manufacturer's protocol.

675 Luminescence was measured on a Tecan infinite M200 microplate reader (TECAN).

676

677 **Immunocytochemistry of viral antigen**

678 Cells were fixed with acetone:methanol (40:60) solution and immunostaining

679 was performed using a monoclonal antibody directed against the spike (S) protein of

34

680   SARS-CoV-2 (1:1500, Sinobiological), which was detected with a peroxidase-

681   conjugated anti-rabbit secondary antibody (1:1,000, Dianova), followed by addition of

682   AEC substrate. The S positive area was scanned and quantified by the Bioreader®

683   7000-F-Z-I microplate reader (Biosys). The results are expressed as percentage of

684   inhibition relative to virus control which received no drug.

685

686   **Immunofluorescence labeling**

687   Cells were fixed with 3% PFA permeabilized with 0.1 % Triton X-100. Prior to

688   primary antibody labeling, cells were blocked with 5% donkey serum in PBS or 1%

689   BSA and 2% goat serum in PBS for 30 minutes at room temperature. Spike (S) protein

690   was detected using a specific antibody (1:1500, Sinobiological) and an Alexa Fluor 488

691   anti-rabbit secondary antibody (1:200, Invitrogen). The nucleus was labeled using

692   DAPI (1:1000, Thermo Scientific). Cardiomyocytes were counterstained with Alexa

693   FluorTM 647 Phalloidin (1:100, #A22287, Invitrogen). Images were taken using

694   Spark® Mulitmode microplate reader (TECAN) at 10x magnification.

695

696   **Immunoblot assay**

697   Cells were lysed using Triton-X-100 sample buffer (Sigma-Aldrich), and proteins

698   were separated by SDS-PAGE. Detection occurred by using specific antibodies

699   against GAPDH (1:1000 dilution, #2275-PC-100, Trevigen), SARS-CoV-2 NP (1:1000

700   dilution, #40143-R019, Sino Biological), ACE2 (1:500 dilution, #ab15348, Abcam), and

701   TMPRSS2 (1:1000 dilution, Recombinant Anti-TMPRSS2 antibody [EPR3861],

702   #ab92323, Abcam) followed by incubation with IRDye-labeled secondary antibodies

703   (LI-COR Biotechnology, IRDye®800CW Goat anti-Rabbit, 926-32211, 1:40,000)

704   according to the manufacturer's instructions. Protein bands were visualized by laser-

35

705   induced fluorescence using an infrared scanner for protein quantification (Odyssey, Li-

706   Cor Biosciences, Bad Homburg, Germany).

707

qRT-PCR

709   SARS-CoV-2 RNA from cell culture supernatant samples was isolated using

710   AVL buffer and the QIAamp Viral RNA Kit (QIAGEN) according to the manufacturer's

711   instructions. Quantification of viral RNA was performed as previously described

712   [Bojkova et al., 2020; Toptan et al., 2020] using primers targeting the RNA-dependent

713   RNA polymerase (RdRp): RdRP_SARSr-F2 (GTG ARA TGG TCA TGT GTG GCG G)

714   and RdRP_SARSr-R1 (CAR ATG TTA AAS ACA CTA TTA GCA TA). Standard curves

715   were created using plasmid DNA (pEX-A128-RdRP) harboring the corresponding

716   amplicon regions for RdRP target sequence according to GenBank Accession number

717   NC_045512. All quantification experiments have been carried out with biological

718   replicates.

719

Neutralization assay

721   Serum of double mRNA-1273-vaccinated individuals was serially diluted and pre-

722   incubated with 4000 TCID50/mL of SARS-CoV-2 variants at 37°C for 1 h prior transfer

723   to Caco-2-F03 monolayers in 96 well plate. The neutralization titer was determined

724   either by visual scoring of CPE 72 h post infection or caspase 3/7 activity

725   measurement.

726

Selection of drug-resistant variant

728   SARS-CoV-2/FFM3 was serially passaged with increasing concentration

729   (starting concentration - 500nM) of remdesivir in Caco-2-F03. Viral replication was

36

730   monitored by observation for any cytopathogenic effect present in the culture. Infected

731   cultures were frozen at −80°C and thawed once prior a passaging. Virus was serially

732   passaged by using 1 aliquot of viral stock from the preceding passage to infect fresh

733   Caco-2-F03 cells (MOI of 0.1) in the presence of increasing concentrations of

734   compound for a total of 30 passages,resulting in a strain that could be readily passaged

735   in the presence of remdesivir 2 µM (FFM3^{r}REM).

736

Sequencing

738   Extracted nucleic acid was DNase treated, reverse transcribed, and randomly

739   amplified using a Sequence-Independent Single-Primer Amplification (SISPA) method

740   described previously [Lewandowski et al., 2019]. Illumina sequencing used the Nextera

741   XT protocol with 2 × 150-bp paired-end sequencing on a MiSeq.

742

Phospholipidosis quantification

744   Phospholipidosis was assessed as previously described [Tummino et al., 2021].

745   Cells were treated with hydroxychloroquine in the presence of 7.5 µM

746   nitrobenzoxadiazole-conjugated phosphoethanolamine (NBD-PE) (ThermoFisher).

747   Images were taken and the fluorescence was quantified using a Spark® Mulitmode

748   microplate reader (TECAN).

749

Screening assay

751   The Kinase inhibitor library L-1200 (Selleckchem) containing 1796 compounds

752   was tested in a proof-of-concept screen in Delta-infected Caco-2-F03 cells for the

753   identification of antivirally active agents. Caco-2-F03 cells were seeded into 96-well

754   plates (50,000 cells/well) and incubated at 37°C for 4 days. After the cells reached

755 confluence, the supernatant was replaced by 25 µL/well of medium containing the

756 ABCB1 inhibitor zosuquidar (final concentration 1 µM), 25 µL/well of medium

757 containing kinase inhibitors (final concentration 10 µM) in singlets, and 50 µL/ well

758 SARS-CoV-2 suspension (MOI 0.01). Remdesivir (10 µM) was used as positive

759 control. Plates were incubated at 37°C for 48h prior to the measurement of caspase

760 3/7 activity as described above. For each plate the Z´ score, a measure of statistical

761 effect size and an index for assay quality control, was calculated by: $Z' = 1 -$

762 $(3*s.d.signal + 3*s.d.basal)/(Mean_{signal} - Mean_{basal})$. Only plates with Z´score ≥ 0.5

763 were further analyzed.

764

765 **Drug combination studies**

766 To evaluate antiviral activity of drug combinations, drugs were tested alone or

767 in fixed combinations at 1:2 dilutions using monolayers of Caco-2-F03 cells infected

768 with the indicated SARS-CoV-2 isolates at MOI 1. Antiviral effects were detected 24 h

769 post infection by immunofluorescence staining for S protein. The calculation of IC50,

770 IC75, IC90 and IC95 for single drugs and their combinations as well as combination

771 indices (CIs) was performed using the software CalcuSyn (Biosoft) based on the

772 method of Chou and Talalay [Chou, 2006]. The weighted average CI value (CI_{wt}) was

773 calculated according to the formula: $CI_{wt} [CI_{50} + 2CI_{75} + 3CI_{90} + 4CI_{95}]/10$. CI_{wt} values

774 were calculated for mutually exclusive interactions where $CI_{wt}<1$ indicates synergism,

775 $CI_{wt} =1$ indicates additive effects, and $CI_{wt} >1$ suggest antagonism.

776

777 **Statistical analysis**

778 The results are expressed as the mean ± standard deviation of at least three

779 experiments. The Student's *t*-test was used for comparing two groups. Three and more

780   groups were compared by ANOVA. GraphPad Prism 9 was used to determine IC50

781   and CC50.

782

783 **References**

784 Agrawal P, Sambaturu N, Olgun G, Hannenhalli S. A path-based analysis of infected

785 cell line and COVID-19 patient transcriptome reveals novel potential targets and drugs

786 against SARS-CoV-2. Res Sq. 2022 Mar 21:rs.3.rs-1474136. doi: 10.21203/rs.3.rs-

787 1474136/v1.

788 Apaydın ÇB, Çınar G, Cihan-Üstündağ G. Small-molecule antiviral agents in ongoing

789 clinical trials for COVID-19. Curr Drug Targets. 2021 Feb 14. doi:

790 10.2174/1389450122666210215112150.

791 Arlt B, Mastrobuoni G, Wuenschel J, Astrahantseff K, Eggert A, Kempa S, Deubzer

792 HE. Inhibiting PHGDH with NCT-503 reroutes glucose-derived carbons into the TCA

793 cycle, independently of its on-target effect. J Enzyme Inhib Med Chem. 2021

794 Dec;36(1):1282-1289. doi: 10.1080/14756366.2021.1935917.

795 Basile MS, Cavalli E, McCubrey J, Hernández-Bello J, Muñoz-Valle JF, Fagone P,

796 Nicoletti F. The PI3K/Akt/mTOR pathway: A potential pharmacological target in

797 COVID-19. Drug Discov Today. 2022 Mar;27(3):848-856. doi:

798 10.1016/j.drudis.2021.11.002.

799 Ben-David U, Siranosian B, Ha G, Tang H, Oren Y, Hinohara K, Strathdee CA,

800 Dempster J, Lyons NJ, Burns R, Nag A, Kugener G, Cimini B, Tsvetkov P, Maruvka

801 YE, O'Rourke R, Garrity A, Tubelli AA, Bandopadhayay P, Tsherniak A, Vazquez F,

802 Wong B, Birger C, Ghandi M, Thorner AR, Bittker JA, Meyerson M, Getz G, Beroukhim

803 R, Golub TR. Genetic and transcriptional evolution alters cancer cell line drug

804 response. Nature. 2018 Aug;560(7718):325-330. doi: 10.1038/s41586-018-0409-3.

805 Bielarz V, Willemart K, Avalosse N, De Swert K, Lotfi R, Lejeune N, Poulain F, Ninanne

806 N, Gilloteaux J, Gillet N, Nicaise C. Susceptibility of neuroblastoma and glioblastoma

807 cell lines to SARS-CoV-2 infection. Brain Res. 2021 May 1;1758:147344. doi:

808 10.1016/j.brainres.2021.147344.

809 Bojkova D, Klann K, Koch B, Widera M, Krause D, Ciesek S, Cinatl J, Münch C.

810 Proteomics of SARS-CoV-2-infected host cells reveals therapy targets. Nature. 2020

811 Jul;583(7816):469-472. doi: 10.1038/s41586-020-2332-7.

812 Bojkova D, Wagner JUG, Shumliakivska M, Aslan GS, Saleem U, Hansen A, Luxán G,

813 Günther S, Pham MD, Krishnan J, Harter PN, Ermel UH, Frangakis AS, Milting H,

814 Zeiher AM, Klingel K, Cinatl J, Dendorfer A, Eschenhagen T, Tschöpe C, Ciesek S,

815 Dimmeler S. SARS-CoV-2 infects and induces cytotoxic effects in human

816 cardiomyocytes. Cardiovasc Res. 2020a Dec 1;116(14):2207-2215. doi:

817 10.1093/cvr/cvaa267.

818 Bojkova D, Bechtel M, McLaughlin KM, McGreig JE, Klann K, Bellinghausen C, Rohde

819 G, Jonigk D, Braubach P, Ciesek S, Münch C, Wass MN, Michaelis M, Cinatl J Jr.

820 Aprotinin Inhibits SARS-CoV-2 Replication. Cells. 2020b Oct 30;9(11):2377. doi:

821 10.3390/cells9112377.

822 Bojkova D, McGreig JE, McLaughlin KM, Masterson SG, Antczak M, Widera M,

823 Krähling V, Ciesek S, Wass MN, Michaelis M, Cinatl J. Differentially conserved amino

824 acid positions may reflect differences in SARS-CoV-2 and SARS-CoV behaviour.

825 Bioinformatics. 2021 Feb 9:btab094. doi: 10.1093/bioinformatics/btab094.

826 Bojkova D, Rothenburger T, Ciesek S, Wass MN, Michaelis M, Cinatl J Jr. SARS-CoV-

827 2 Omicron variant virus isolates are highly sensitive to interferon treatment. Cell

828 Discov. 2022 May 10;8(1):42. doi: 10.1038/s41421-022-00408-z.

829 Breckwoldt K, Letuffe-Brenière D, Mannhardt I, Schulze T, Ulmer B, Werner T, Benzin

830 A, Klampe B, Reinsch MC, Laufer S, Shibamiya A, Prondzynski M, Mearini G, Schade

831 D, Fuchs S, Neuber C, Krämer E, Saleem U, Schulze ML, Rodriguez ML,

832 Eschenhagen T, Hansen A. Differentiation of cardiomyocytes and generation of human

833 engineered heart tissue. Nat Protoc. 2017 Jun;12(6):1177-1197. doi:

834 10.1038/nprot.2017.033.

835   Caccuri F, Zani A, Messali S, Giovanetti M, Bugatti A, Campisi G, Filippini F, Scaltriti
836   E, Ciccozzi M, Fiorentini S, Caruso A. A persistently replicating SARS-CoV-2 variant
837   derived from an asymptomatic individual. J Transl Med. 2020 Sep 23;18(1):362. doi:
838   10.1186/s12967-020-02535-1.

839   Chan JF, Chan KH, Choi GK, To KK, Tse H, Cai JP, Yeung ML, Cheng VC, Chen H,
840   Che XY, Lau SK, Woo PC, Yuen KY. Differential cell line susceptibility to the emerging
841   novel human betacoronavirus 2c EMC/2012: implications for disease pathogenesis
842   and clinical manifestation. J Infect Dis. 2013 Jun 1;207(11):1743-52. doi:
843   10.1093/infdis/jit123.

844   Chan KH, Yan MK, To KK, Lau SK, Woo PC, Cheng VC, Li WS, Chan JF, Tse H, Yuen
845   KY. Use of the human colorectal adenocarcinoma (Caco-2) cell line for isolating
846   respiratory viruses from nasopharyngeal aspirates. J Med Virol. 2013a May;85(5):874-
847   9. doi: 10.1002/jmv.23538.

848   Chou TC. Theoretical basis, experimental design, and computerized simulation of
849   synergism and antagonism in drug combination studies. Pharmacol Rev. 2006
850   Sep;58(3):621-81. doi: 10.1124/pr.58.3.10.

851   Chu H, Chan JF, Yuen TT, Shuai H, Yuan S, Wang Y, Hu B, Yip CC, Tsang JO, Huang
852   X, Chai Y, Yang D, Hou Y, Chik KK, Zhang X, Fung AY, Tsoi HW, Cai JP, Chan WM,
853   Ip JD, Chu AW, Zhou J, Lung DC, Kok KH, To KK, Tsang OT, Chan KH, Yuen KY.
854   Comparative tropism, replication kinetics, and cell damage profiling of SARS-CoV-2
855   and SARS-CoV with implications for clinical manifestations, transmissibility, and
856   laboratory studies of COVID-19: an observational study. Lancet Microbe. 2020
857   May;1(1):e14-e23. doi: 10.1016/S2666-5247(20)30004-5.

858   Cinatl J, Morgenstern B, Bauer G, Chandra P, Rabenau H, Doerr HW. Treatment of
859   SARS with human interferons. Lancet. 2003 Jul 26;362(9380):293-4. doi:
860   10.1016/s0140-6736(03)13973-6.

861   Cinatl J Jr, Hoever G, Morgenstern B, Preiser W, Vogel JU, Hofmann WK, Bauer G,

862   Michaelis M, Rabenau HF, Doerr HW. Infection of cultured intestinal epithelial cells

863   with severe acute respiratory syndrome coronavirus. Cell Mol Life Sci. 2004

864   Aug;61(16):2100-12. doi: 10.1007/s00018-004-4222-9.

865   Collins AR. Comparison of the replication of distinct strains of human coronavirus

866   OC43 in organotypic human colon cells (Caco-2) and mouse intestine. Adv Exp Med

867   Biol. 1990;276:497-503. doi: 10.1007/978-1-4684-5823-7_69.

868   Connolly PF, Fearnhead HO. Viral hijacking of host caspases: an emerging category

869   of pathogen-host interactions. Cell Death Differ. 2017 Aug;24(8):1401-1410. doi:

870   10.1038/cdd.2017.59.

871   Dittmar M, Lee JS, Whig K, Segrist E, Li M, Kamalia B, Castellana L, Ayyanathan K,

872   Cardenas-Diaz FL, Morrisey EE, Truitt R, Yang W, Jurado K, Samby K, Ramage H,

873   Schultz DC, Cherry S. Drug repurposing screens reveal cell-type-specific entry

874   pathways and FDA-approved drugs active against SARS-Cov-2. Cell Rep. 2021 Apr

875   6;35(1):108959. doi: 10.1016/j.celrep.2021.108959.

876   Ellinger B, Bojkova D, Zaliani A, Cinatl J, Claussen C, Westhaus S, Keminer O,

877   Reinshagen J, Kuzikov M, Wolf M, Geisslinger G, Gribbon P, Ciesek S. A SARS-CoV-

878   2 cytopathicity dataset generated by high-content screening of a large drug

879   repurposing collection. Sci Data. 2021 Feb 26;8(1):70. doi: 10.1038/s41597-021-

880   00848-4.

881   Feichtinger J, Hernández I, Fischer C, Hanscho M, Auer N, Hackl M, Jadhav V,

882   Baumann M, Krempl PM, Schmidl C, Farlik M, Schuster M, Merkel A, Sommer A, Heath

883   S, Rico D, Bock C, Thallinger GG, Borth N. Comprehensive genome and epigenome

884   characterization of CHO cells in response to evolutionary pressures and over time.

885   Biotechnol Bioeng. 2016 Oct;113(10):2241-53. doi: 10.1002/bit.25990.

886   Fogh J, Fogh JM, Orfeo T. One hundred and twenty-seven cultured human tumor cell

887   lines producing tumors in nude mice. J Natl Cancer Inst. 1977 Jul;59(1):221-6. doi:

888   10.1093/jnci/59.1.221.

889   Gao J, Sun F. Drug discovery to treat COVID-19 two years after its outbreak. Drug

890   Discov Ther. 2021;15(6):281-288. doi: 10.5582/ddt.2021.01302.

891   Garcia G Jr, Sharma A, Ramaiah A, Sen C, Purkayastha A, Kohn DB, Parcells MS,

892   Beck S, Kim H, Bakowski MA, Kirkpatrick MG, Riva L, Wolff KC, Han B, Yuen C, Ulmert

893   D, Purbey PK, Scumpia P, Beutler N, Rogers TF, Chatterjee AK, Gabriel G,

894   Bartenschlager R, Gomperts B, Svendsen CN, Betz UAK, Damoiseaux RD,

895   Arumugaswami V. Antiviral drug screen identifies DNA-damage response inhibitor as

896   potent blocker of SARS-CoV-2 replication. Cell Rep. 2021 Apr 6;35(1):108940. doi:

897   10.1016/j.celrep.2021.108940.

898   Gentile I, Schiano Moriello N. COVID-19 prophylaxis in immunosuppressed patients:

899   Beyond vaccination. PLoS Med. 2022 Jan 28;19(1):e1003917. doi:

900   10.1371/journal.pmed.1003917.

901   Geeraerts SL, Heylen E, De Keersmaecker K, Kampen KR. The ins and outs of serine

902   and glycine metabolism in cancer. Nat Metab. 2021 Feb;3(2):131-141. doi:

903   10.1038/s42255-020-00329-9.

904   Gower G, Picazo PI, Fumagalli M, Racimo F. Detecting adaptive introgression in

905   human evolution using convolutional neural networks. Elife. 2021 May 25;10:e64669.

906   doi: 10.7554/eLife.64669.

907   Gutierrez-Chamorro L, Felip E, Ezeonwumelu IJ, Margelí M, Ballana E. Cyclin-

908   dependent Kinases as Emerging Targets for Developing Novel Antiviral Therapeutics.

909   Trends Microbiol. 2021 Sep;29(9):836-848. doi: 10.1016/j.tim.2021.01.014.

910   Hahn F, Hamilton ST, Wangen C, Wild M, Kicuntod J, Brückner N, Follett JEL,

911   Herrmann L, Kheimar A, Kaufer BB, Rawlinson WD, Tsogoeva SB, Marschall M.

912   Development of a PROTAC-Based Targeting Strategy Provides a Mechanistically

913   Unique Mode of Anti-Cytomegalovirus Activity. Int J Mol Sci. 2021 Nov

914   27;22(23):12858. doi: 10.3390/ijms222312858.

915   Hamanaka RB, Nigdelioglu R, Meliton AY, Tian Y, Witt LJ, O'Leary E, Sun KA, Woods

916   PS, Wu D, Ansbro B, Ard S, Rohde JM, Dulin NO, Guzy RD, Mutlu GM. Inhibition of

917   Phosphoglycerate Dehydrogenase Attenuates Bleomycin-induced Pulmonary

918   Fibrosis. Am J Respir Cell Mol Biol. 2018 May;58(5):585-593. doi: 10.1165/rcmb.2017-

919   0186OC.

920   He X, Quan S, Xu M, Rodriguez S, Goh SL, Wei J, Fridman A, Koeplinger KA, Carroll

921   SS, Grobler JA, Espeseth AS, Olsen DB, Hazuda DJ, Wang D. Generation of SARS-

922   CoV-2 reporter replicon for high-throughput antiviral screening and testing. Proc Natl

923   Acad Sci U S A. 2021 Apr 13;118(15):e2025866118. doi: 10.1073/pnas.2025866118.

924   Hiscox JA, Khoo SH, Stewart JP, Owen A. Shutting the gate before the horse has

925   bolted: is it time for a conversation about SARS-CoV-2 and antiviral drug resistance?

926   J Antimicrob Chemother. 2021 Aug 12;76(9):2230-2233. doi: 10.1093/jac/dkab189.

927   Hoehl S, Rabenau H, Berger A, Kortenbusch M, Cinatl J, Bojkova D, Behrens P,

928   Böddinghaus B, Götsch U, Naujoks F, Neumann P, Schork J, Tiarks-Jungk P, Walczok

929   A, Eickmann M, Vehreschild MJGT, Kann G, Wolf T, Gottschalk R, Ciesek S. Evidence

930   of SARS-CoV-2 Infection in Returning Travelers from Wuhan, China. N Engl J Med.

931   2020 Mar 26;382(13):1278-1280. doi: 10.1056/NEJMc2001899.

932   Jamaly S, Tsokos MG, Bhargava R, Brook OR, Hecht JL, Abdi R, Moulton VR, Satyam

933   A, Tsokos GC. Complement activation and increased expression of Syk, mucin-1 and

934   CaMK4 in kidneys of patients with COVID-19. Clin Immunol. 2021 Aug;229:108795.

935   doi: 10.1016/j.clim.2021.108795.

936 Klann K, Bojkova D, Tascher G, Ciesek S, Münch C, Cinatl J. Growth Factor Receptor

937 Signaling Inhibition Prevents SARS-CoV-2 Replication. Mol Cell. 2020 Oct

938 1;80(1):164-174.e4. doi: 10.1016/j.molcel.2020.08.006.

939 Lee S, Yoon GY, Myoung J, Kim SJ, Ahn DG. Robust and persistent SARS-CoV-2

940 infection in the human intestinal brush border expressing cells. Emerg Microbes Infect.

941 2020 Dec;9(1):2169-2179. doi: 10.1080/22221751.2020.1827985.

942 Lewandowski K, Xu Y, Pullan ST, Lumley SF, Foster D, Sanderson N, Vaughan A,

943 Morgan M, Bright N, Kavanagh J, Vipond R, Carroll M, Marriott AC, Gooch KE,

944 Andersson M, Jeffery K, Peto TEA, Crook DW, Walker AS, Matthews PC.

945 Metagenomic Nanopore Sequencing of Influenza Virus Direct from Clinical Respiratory

946 Samples. J Clin Microbiol. 2019 Dec 23;58(1):e00963-19. doi: 10.1128/JCM.00963-

947 19.

948 Li S, Zhang Y, Guan Z, Li H, Ye M, Chen X, Shen J, Zhou Y, Shi ZL, Zhou P, Peng K.

949 SARS-CoV-2 triggers inflammatory responses and cell death through caspase-8

950 activation. Signal Transduct Target Ther. 2020 Oct 9;5(1):235. doi: 10.1038/s41392-

951 020-00334-0.

952 Liao Y, Li X, Mou T, Zhou X, Li D, Wang L, Zhang Y, Dong X, Zheng H, Guo L, Liang

953 Y, Jiang G, Fan S, Xu X, Xie Z, Chen H, Liu L, Li Q. Distinct infection process of SARS-

954 CoV-2 in human bronchial epithelial cell lines. J Med Virol. 2020 Nov;92(11):2830-

955 2838. doi: 10.1002/jmv.26200.

956 Liu Y, Mi Y, Mueller T, Kreibich S, Williams EG, Van Drogen A, Borel C, Frank M,

957 Germain PL, Bludau I, Mehnert M, Seifert M, Emmenlauer M, Sorg I, Bezrukov F, Bena

958 FS, Zhou H, Dehio C, Testa G, Saez-Rodriguez J, Antonarakis SE, Hardt WD,

959 Aebersold R. Multi-omic measurements of heterogeneity in HeLa cells across

960 laboratories. Nat Biotechnol. 2019 Mar;37(3):314-322. doi: 10.1038/s41587-019-0037-

961 y.

962 Michaelis M, Doerr HW, Cinatl J Jr. Investigation of the influence of EPs® 7630, a
963 herbal drug preparation from Pelargonium sidoides, on replication of a broad panel of
964 respiratory viruses. Phytomedicine. 2011 Mar 15;18(5):384-6. doi:
965 10.1016/j.phymed.2010.09.008.

966 Mulay A, Konda B, Garcia G Jr, Yao C, Beil S, Villalba JM, Koziol C, Sen C,
967 Purkayastha A, Kolls JK, Pociask DA, Pessina P, de Aja JS, Garcia-de-Alba C, Kim
968 CF, Gomperts B, Arumugaswami V, Stripp BR. SARS-CoV-2 infection of primary
969 human lung epithelium for COVID-19 modeling and drug discovery. Cell Rep. 2021
970 May 4;35(5):109055. doi: 10.1016/j.celrep.2021.109055.

971 Ogando NS, Dalebout TJ, Zevenhoven-Dobbe JC, Limpens RWAL, van der Meer Y,
972 Caly L, Druce J, de Vries JJC, Kikkert M, Bárcena M, Sidorov I, Snijder EJ. SARS-
973 coronavirus-2 replication in Vero E6 cells: replication kinetics, rapid adaptation and
974 cytopathology. J Gen Virol. 2020 Sep;101(9):925-940. doi: 10.1099/jgv.0.001453.

975 Pacold ME, Brimacombe KR, Chan SH, Rohde JM, Lewis CA, Swier LJ, Possemato
976 R, Chen WW, Sullivan LB, Fiske BP, Cho S, Freinkman E, Birsoy K, Abu-Remaileh M,
977 Shaul YD, Liu CM, Zhou M, Koh MJ, Chung H, Davidson SM, Luengo A, Wang AQ,
978 Xu X, Yasgar A, Liu L, Rai G, Westover KD, Vander Heiden MG, Shen M, Gray NS,
979 Boxer MB, Sabatini DM. A PHGDH inhibitor reveals coordination of serine synthesis
980 and one-carbon unit fate. Nat Chem Biol. 2016 Jun;12(6):452-8. doi:
981 10.1038/nchembio.2070.

982 Pajak B, Siwiak E, Sołtyka M, Priebe A, Zieliński R, Fokt I, Ziemniak M, Jaśkiewicz A,
983 Borowski R, Domoradzki T, Priebe W. 2-Deoxy-d-Glucose and Its Analogs: From
984 Diagnostic to Therapeutic Agents. Int J Mol Sci. 2019 Dec 29;21(1):234. doi:
985 10.3390/ijms21010234.

986 Ramani R, Laplante JM, Church TM, Farrell GM, Lamson DM, St George K. CACO-2
987 cells: A continuous cell line with sensitive and broad-spectrum utility for respiratory

988   virus culture. J Virol Methods. 2021 Jul;293:114120. doi: 10.1016/j.jviromet.2021.114120.

989

990   Ramirez S, Fernandez-Antunez C, Galli A, Underwood A, Pham LV, Ryberg LA, Feng

991   S, Pedersen MS, Mikkelsen LS, Belouzard S, Dubuisson J, Sølund C, Weis N,

992   Gottwein JM, Fahnøe U, Bukh J. Overcoming Culture Restriction for SARS-CoV-2 in

993   Human Cells Facilitates the Screening of Compounds Inhibiting Viral Replication.

994   Antimicrob Agents Chemother. 2021 Jun 17;65(7):e0009721. doi:

995   10.1128/AAC.00097-21.

996   Reid MA, Allen AE, Liu S, Liberti MV, Liu P, Liu X, Dai Z, Gao X, Wang Q, Liu Y, Lai L,

997   Locasale JW. Serine synthesis through PHGDH coordinates nucleotide levels by

998   maintaining central carbon metabolism. Nat Commun. 2018 Dec 21;9(1):5442. doi:

999   10.1038/s41467-018-07868-6.

1000 Reigel F. Isolation of human pathogenic viruses from clinical material on CaCo2 cells.

1001 J Virol Methods. 1985 Dec;12(3-4):323-7. doi: 10.1016/0166-0934(85)90143-0.

1002 Ren Y, Shu T, Wu D, Mu J, Wang C, Huang M, Han Y, Zhang XY, Zhou W, Qiu Y,

1003 Zhou X. The ORF3a protein of SARS-CoV-2 induces apoptosis in cells. Cell Mol

1004 Immunol. 2020 Aug;17(8):881-883. doi: 10.1038/s41423-020-0485-9.

1005 Riva L, Yuan S, Yin X, Martin-Sancho L, Matsunaga N, Pache L, Burgstaller-

1006 Muehlbacher S, De Jesus PD, Teriete P, Hull MV, Chang MW, Chan JF, Cao J, Poon

1007 VK, Herbert KM, Cheng K, Nguyen TH, Rubanov A, Pu Y, Nguyen C, Choi A,

1008 Rathnasinghe R, Schotsaert M, Miorin L, Dejosez M, Zwaka TP, Sit KY, Martinez-

1009 Sobrido L, Liu WC, White KM, Chapman ME, Lendy EK, Glynne RJ, Albrecht R, Ruppin

1010 E, Mesecar AD, Johnson JR, Benner C, Sun R, Schultz PG, Su AI, García-Sastre A,

1011 Chatterjee AK, Yuen KY, Chanda SK. Discovery of SARS-CoV-2 antiviral drugs

1012 through large-scale compound repurposing. Nature. 2020 Oct;586(7827):113-119. doi:

1013 10.1038/s41586-020-2577-1.

1014   Sahu KK, Kumar R. Role of 2-Deoxy-D-Glucose (2-DG) in COVID-19 disease: A

1015   potential game-changer. J Family Med Prim Care. 2021 Oct;10(10):3548-3552. doi:

1016   10.4103/jfmpc.jfmpc_1338_21.

1017   Shahinozzaman M, Basak B, Emran R, Rozario P, Obanda DN. Artepillin C: A

1018   comprehensive review of its chemistry, bioavailability, and pharmacological properties.

1019   Fitoterapia. 2020 Nov;147:104775. doi: 10.1016/j.fitote.2020.104775.

1020   Shang C, Zhuang X, Zhang H, Li Y, Zhu Y, Lu J, Ge C, Cong J, Li T, Li N, Tian M, Jin

1021   N, Li X. Inhibition of Autophagy Suppresses SARS-CoV-2 Replication and Ameliorates

1022   Pneumonia in hACE2 Transgenic Mice and Xenografted Human Lung Tissues. J Virol.

1023   2021 Nov 23;95(24):e0153721. doi: 10.1128/JVI.01537-21.

1024   Shiffman ML, Pockros P, McHutchison JG, Schiff ER, Morris M, Burgess G. Clinical

1025   trial: the efficacy and safety of oral PF-03491390, a pancaspase inhibitor - a

1026   randomized placebo-controlled study in patients with chronic hepatitis C. Aliment

1027   Pharmacol Ther. 2010 May;31(9):969-78. doi: 10.1111/j.1365-2036.2010.04264.x.

1028   Simonis A, Theobald SJ, Fätkenheuer G, Rybniker J, Malin JJ. A comparative analysis

1029   of remdesivir and other repurposed antivirals against SARS-CoV-2. EMBO Mol Med.

1030   2021 Jan 11;13(1):e13105. doi: 10.15252/emmm.202013105.

1031   Szemiel AM, Merits A, Orton RJ, MacLean OA, Pinto RM, Wickenhagen A, Lieber G,

1032   Turnbull ML, Wang S, Furnon W, Suarez NM, Mair D, da Silva Filipe A, Willett BJ,

1033   Wilson SJ, Patel AH, Thomson EC, Palmarini M, Kohl A, Stewart ME. In vitro selection

1034   of Remdesivir resistance suggests evolutionary predictability of SARS-CoV-2. PLoS

1035   Pathog. 2021 Sep 17;17(9):e1009929. doi: 10.1371/journal.ppat.1009929.

1036   Tang BS, Chan KH, Cheng VC, Woo PC, Lau SK, Lam CC, Chan TL, Wu AK, Hung

1037   IF, Leung SY, Yuen KY. Comparative host gene transcription by microarray analysis

1038   early after infection of the Huh7 cell line by severe acute respiratory syndrome

1039   coronavirus and human coronavirus 229E. J Virol. 2005 May;79(10):6180-93. doi:

1040   10.1128/JVI.79.10.6180-6193.2005.

1041   Thi Nhu Thao T, Labroussaa F, Ebert N, V'kovski P, Stalder H, Portmann J, Kelly J,

1042   Steiner S, Holwerda M, Kratzel A, Gultom M, Schmied K, Laloli L, Hüsser L, Wider M,

1043   Pfaender S, Hirt D, Cippà V, Crespo-Pomar S, Schröder S, Muth D, Niemeyer D,

1044   Corman VM, Müller MA, Drosten C, Dijkman R, Jores J, Thiel V. Rapid reconstruction

1045   of SARS-CoV-2 using a synthetic genomics platform. Nature. 2020

1046   Jun;582(7813):561-565. doi: 10.1038/s41586-020-2294-9.

1047   Toptan T, Hoehl S, Westhaus S, Bojkova D, Berger A, Rotter B, Hoffmeier K, Cinatl J

1048   Jr, Ciesek S, Widera M. Optimized qRT-PCR Approach for the Detection of Intra- and

1049   Extra-Cellular SARS-CoV-2 RNAs. Int J Mol Sci. 2020 Jun 20;21(12):4396. doi:

1050   10.3390/ijms21124396.

1051   Touret F, Gilles M, Barral K, Nougairède A, van Helden J, Decroly E, de Lamballerie

1052   X, Coutard B. In vitro screening of a FDA approved chemical library reveals potential

1053   inhibitors of SARS-CoV-2 replication. Sci Rep. 2020 Aug 4;10(1):13093. doi:

1054   10.1038/s41598-020-70143-6.

1055   Tummino TA, Rezelj VV, Fischer B, Fischer A, O'Meara MJ, Monel B, Vallet T, White

1056   KM, Zhang Z, Alon A, Schadt H, O'Donnell HR, Lyu J, Rosales R, McGovern BL,

1057   Rathnasinghe R, Jangra S, Schotsaert M, Galarneau JR, Krogan NJ, Urban L, Shokat

1058   KM, Kruse AC, García-Sastre A, Schwartz O, Moretti F, Vignuzzi M, Pognan F,

1059   Shoichet BK. Drug-induced phospholipidosis confounds drug repurposing for SARS-

1060   CoV-2. Science. 2021 Jul 30;373(6554):541-547. doi: 10.1126/science.abi4708.

1061   Van Damme E, De Meyer S, Bojkova D, Ciesek S, Cinatl J, De Jonghe S, Jochmans

1062   D, Leyssen P, Buyck C, Neyts J, Van Loock M. In vitro activity of itraconazole against

1063   SARS-CoV-2. J Med Virol. 2021 Jul;93(7):4454-4460. doi: 10.1002/jmv.26917.

1064   van Wetering S, van der Linden AC, van Sterkenburg MA, de Boer WI, Kuijpers AL,

1065   Schalkwijk J, Hiemstra PS. Regulation of SLPI and elafin release from bronchial

1066   epithelial cells by neutrophil defensins. Am J Physiol Lung Cell Mol Physiol. 2000

1067   Jan;278(1):L51-8. doi: 10.1152/ajplung.2000.278.1.L51.

1068   Vondran FW, Katenz E, Schwartlander R, Morgul MH, Raschzok N, Gong X, Cheng

1069   X, Kehr D, Sauer IM. Isolation of primary human hepatocytes after partial hepatectomy:

1070   criteria for identification of the most promising liver specimen. Artif Organs. 2008

1071   Mar;32(3):205-13. doi: 10.1111/j.1525-1594.2007.00524.x.

1072   White JM, Schiffer JT, Bender Ignacio RA, Xu S, Kainov D, Ianevski A, Aittokallio T,

1073   Frieman M, Olinger GG, Polyak SJ. Drug Combinations as a First Line of Defense

1074   against Coronaviruses and Other Emerging Viruses. mBio. 2021 Dec

1075   21;12(6):e0334721. doi: 10.1128/mbio.03347-21.

1076   Widera M, Mühlemann B, Corman VM, Toptan T, Beheim-Schwarzbach J, Kohmer N,

1077   Schneider J, Berger A, Veith T, Pallas C, Bleicker T, Goetsch U, Tesch J, Gottschalk

1078   R, Jones TC, Ciesek S, Drosten C. Surveillance of SARS-CoV-2 in Frankfurt am Main

1079   from October to December 2020 Reveals High Viral Diversity Including Spike Mutation

1080   N501Y in B.1.1.70 and B.1.1.7. Microorganisms. 2021 Apr 2;9(4):748. doi:

1081   10.3390/microorganisms9040748.

1082   Wurtz N, Penant G, Jardot P, Duclos N, La Scola B. Culture of SARS-CoV-2 in a panel

1083   of laboratory cell lines, permissivity, and differences in growth profile. Eur J Clin

1084   Microbiol Infect Dis. 2021 Mar;40(3):477-484. doi: 10.1007/s10096-020-04106-0.

1085   Xie X, Muruato AE, Zhang X, Lokugamage KG, Fontes-Garfias CR, Zou J, Liu J, Ren

1086   P, Balakrishnan M, Cihlar T, Tseng CK, Makino S, Menachery VD, Bilello JP, Shi PY.

1087   A nanoluciferase SARS-CoV-2 for rapid neutralization testing and screening of anti-

1088   infective drugs for COVID-19. Nat Commun. 2020 Oct 15;11(1):5214. doi:

1089   10.1038/s41467-020-19055-7.

1090   Yan K, Rawle DJ, Le TT, Suhrbier A. Simple rapid in vitro screening method for SARS-

1091   CoV-2 anti-virals that identifies potential cytomorbidity-associated false positives. Virol

1092   J. 2021a Jun 9;18(1):123. doi: 10.1186/s12985-021-01587-z.

1093   Yang KS, Leeuwon SZ, Xu S, Liu WR. Evolutionary and Structural Insights about

1094   Potential SARS-CoV-2 Evasion of Nirmatrelvir. J Med Chem. 2022 Jun

1095   22:acs.jmedchem.2c00404. doi: 10.1021/acs.jmedchem.2c00404.

1096   Yeung ML, Teng JLL, Jia L, Zhang C, Huang C, Cai JP, Zhou R, Chan KH, Zhao H,

1097   Zhu L, Siu KL, Fung SY, Yung S, Chan TM, To KK, Chan JF, Cai Z, Lau SKP, Chen

1098   Z, Jin DY, Woo PCY, Yuen KY. Soluble ACE2-mediated cell entry of SARS-CoV-2 via

1099   interaction with proteins related to the renin-angiotensin system. Cell. 2021 Apr

1100   15;184(8):2212-2228.e12. doi: 10.1016/j.cell.2021.02.053.

1101   Yoshikawa T, Hill TE, Yoshikawa N, Popov VL, Galindo CL, Garner HR, Peters CJ,

1102   Tseng CT. Dynamic innate immune responses of human bronchial epithelial cells to

1103   severe acute respiratory syndrome-associated coronavirus infection. PLoS One. 2010

1104   Jan 15;5(1):e8729. doi: 10.1371/journal.pone.0008729.

1105   Zhang JH, Chung TD, Oldenburg KR. A Simple Statistical Parameter for Use in

1106   Evaluation and Validation of High Throughput Screening Assays. J Biomol Screen.

1107   1999;4(2):67-73. doi: 10.1177/108705719900400206.

1108   Zhang ZR, Zhang YN, Li XD, Zhang HQ, Xiao SQ, Deng F, Yuan ZM, Ye HQ, Zhang

1109   B. A cell-based large-scale screening of natural compounds for inhibitors of SARS-

1110   CoV-2. Signal Transduct Target Ther. 2020 Oct 3;5(1):218. doi: 10.1038/s41392-020-

1111   00343-z.

1112   Zhang Y, Banga Ndzouboukou JL, Gan M, Lin X, Fan X. Immune Evasive Effects of

1113   SARS-CoV-2 Variants to COVID-19 Emergency Used Vaccines. Front Immunol. 2021

1114   Nov 22;12:771242. doi: 10.3389/fimmu.2021.771242.

1115   Zhang C, Li W, Lei X, Xie Z, Qi L, Wang H, Xiao X, Xiao J, Zheng Y, Dong C, Zheng

1116   X, Chen S, Chen J, Sun B, Qin J, Zhai Q, Li J, Wei B, Wang J, Wang H. Targeting

1117   lysophospholipid acid receptor 1 and ROCK kinases promotes antiviral innate

1118   immunity. Sci Adv. 2021a Sep 17;7(38):eabb5933. doi: 10.1126/sciadv.abb5933.

1119   Zhao H, Lu L, Peng Z, Chen LL, Meng X, Zhang C, Ip JD, Chan WM, Chu AW, Chan

1120   KH, Jin DY, Chen H, Yuen KY, To KK. SARS-CoV-2 Omicron variant shows less

1121   efficient replication and fusion activity when compared with Delta variant in TMPRSS2-

1122   expressed cells. Emerg Microbes Infect. 2022 Dec;11(1):277-283. doi:

1123   10.1080/22221751.2021.2023329.

1124

1125

1126